

## ORIGINAL ARTICLE

# Olfactory Information Storage Engages Subcortical and Cortical Brain Regions That Support Valence Determination

Christina Strauch<sup>1</sup>, Thu-Huong Hoang<sup>1</sup>, Frank Angenstein<sup>2,3,4</sup>  and Denise Manahan-Vaughan<sup>1</sup>

<sup>1</sup>Department of Neurophysiology, Medical Faculty, Ruhr University Bochum, 44780 Bochum, Germany, <sup>2</sup>Functional Neuroimaging Group, Deutsches Zentrum für Neurodegenerative Erkrankungen (DZNE), 39118 Magdeburg, Germany, <sup>3</sup>Leibniz Institute for Neurobiology, 39118 Magdeburg, Germany and <sup>4</sup>Medical Faculty, Otto-von Guericke University, 39118 Magdeburg, Germany

Address correspondence to Denise Manahan-Vaughan, Department of Neurophysiology, Medical Faculty, Ruhr University Bochum, MA 4/150, Universitaetsstr. 150, 44780 Bochum, Germany. Email: [dmv-ign@rub.de](mailto:dmv-ign@rub.de)

## Abstract

The olfactory bulb (OB) delivers sensory information to the piriform cortex (PC) and other components of the olfactory system. OB-PC synapses have been reported to express short-lasting forms of synaptic plasticity, whereas long-term potentiation (LTP) of the anterior PC (aPC) occurs predominantly by activating inputs from the prefrontal cortex. This suggests that brain regions outside the olfactory system may contribute to olfactory information processing and storage. Here, we compared functional magnetic resonance imaging BOLD responses triggered during 20 or 100 Hz stimulation of the OB. We detected BOLD signal increases in the anterior olfactory nucleus (AON), PC and entorhinal cortex, nucleus accumbens, dorsal striatum, ventral diagonal band of Broca, prelimbic–infralimbic cortex (PrL-IL), dorsal medial prefrontal cortex, and basolateral amygdala. Significantly stronger BOLD responses occurred in the PrL-IL, PC, and AON during 100 Hz compared with 20 Hz OB stimulation. LTP in the aPC was concomitantly induced by 100 Hz stimulation. Furthermore, 100 Hz stimulation triggered significant nuclear immediate early gene expression in aPC, AON, and PrL-IL. The involvement of the PrL-IL in this process is consistent with its putative involvement in modulating behavioral responses to odor experience. Furthermore, these results indicate that OB-mediated information storage by the aPC is embedded in a connectome that supports valence evaluation.

**Key words:** fMRI, immediate early gene, olfactory system, prelimbic cortex, synaptic plasticity

## Introduction

During olfactory learning, rodents rapidly categorize odors into appetitive or aversive stimuli (Schoenbaum et al. 1998, 1999; Martin et al. 2004; Chapuis et al. 2009), a process that is underpinned by associative learning (Schoenbaum et al. 1998; Martin et al. 2004; Calu et al. 2007; Roesch et al. 2007; Chapuis et al. 2009). Odor categorization is supported by the orbitofrontal cortex (Schoenbaum and Eichenbaum 1995; Stalnaker et al. 2014; Qu et al. 2016), but this structure, in turn, receives instruction

from subcortical and cortical structures that provide key information about the precise nature of the odor. Here, systems involved in reward and aversive information processing, as well as the integration of sensory modalities, are likely to play a role (Schoenbaum et al. 1999; Schoenbaum and Setlow 2003; Chapuis et al. 2009).

A primary route for the delivery of olfactory information from the olfactory bulb (OB) to the brain is the lateral olfactory tract projection to the olfactory cortex, including the anterior

olfactory nucleus (AON) and piriform cortex (PC) (White 1965; Price 1973). Although David Marr postulated that the piriform cortex shares properties with the hippocampus (Marr 1971), it has recently emerged that, in contrast to the hippocampus, the OB-anterior PC (aPC) pathway does not readily express synaptic plasticity in freely behaving rodents (Strauch and Manahan-Vaughan 2018). Rather, it may be the case that long-term information encoding in the aPC is supported by brain structures outside of the olfactory system. For example, stimulation of the orbitofrontal cortex, a part of the prefrontal cortex that supports information categorization, results in an increase in immediate early gene expression, as well as in long-term potentiation (LTP) in the aPC that lasts for over 4 h (Strauch and Manahan-Vaughan 2018). There is no doubt that the piriform cortex engages in olfactory learning (Roman et al. 1987; Saar et al. 1998; Chapuis and Wilson 2011; Cohen et al. 2015) and that this is supported by changes in excitability within structures of the olfactory system (Cohen et al. 2015). The piriform cortex, in turn, can instruct the hippocampus to store information generated by the aPC by means of synaptic plasticity (Strauch and Manahan-Vaughan 2020). Thus, the question rises as to how robust encoding of olfactory experience results from information transmission from the OB to the brain.

Combining functional magnetic resonance imaging (fMRI) with electrophysiology is a helpful tool to correlate changes in neuronal activity with changes in blood oxygenation level-dependent (BOLD) responses through combined fMRI and *in vivo* electrophysiology in rodents (Angenstein et al. 2007, 2009, 2010; Canals et al. 2009; Bovet-Carmona et al. 2019). Changes in BOLD responses can be correlated to the neural input in combination with the local processing in the target regions (Angenstein et al. 2007, 2010). So far, this type of experimental design has not been used to study the olfactory system from the perspective of information flow from the OB triggered by electrophysiological stimulation. The majority of studies that used fMRI to examine olfactory information processing examined effects of odor presentation. Here, several studies revealed changes in BOLD fMRI in the OB and its layers during odorant stimulation (e.g., Yang et al. 1998; Xu et al. 2000; Schafer et al. 2005; Martin et al. 2007; Li et al. 2014). A few studies examined regions triggered by odor perception using fMRI (Kulkarni et al. 2012; Lehallier et al. 2012; Zhao et al. 2016, 2017; Han et al. 2019; Muir et al. 2019) and some of these demonstrated that odor presentation changed BOLD responses in the AON or PC (Zhao et al. 2016, 2017), while other studies revealed odor- or task-specific changes in BOLD responses during odor stimulation or learning in many regions of the rodent brain (Kulkarni et al. 2012; Han et al. 2019; Muir et al. 2019). Another study using fMRI compared changes in BOLD responses to local field potentials recorded in the aPC and revealed state-dependent functional connectivity in the olfactory system (Wilson et al. 2011).

In this study, our aim was to investigate how electrophysiological emulation of information transmission from the OB to the aPC impacts on subcortical and cortical structures of the brain. We used fMRI to detect cortical and subcortical structures that responded to OB stimulation and identified structures that particularly respond to LTP induction in OB-aPC synapses. These highly responsive structures were then scrutinized further using fluorescence *in situ* hybridization analysis to determine if somatic immediate early gene expression occurred, indicating that information encoding had been triggered. We report that OB activity triggers conjunctive activation of olfactory structures and of brain structures involved in valence evaluation and

the associated encoding of aversive and appetitive experience. This is likely to reflect processes engaged in the interpretation of odor experience and the generation of odor response behaviors.

## Material and Methods

### Subjects

The study was carried out in accordance with the European Communities Council Directive of 22 September 2010 (2010/63/EU), for care of laboratory animals, and all experiments were conducted according to the guidelines of the German Animal Protection Law and were approved by the North Rhine-Westphalia State authority (Bezirksamt, Arnsberg) and the State authority of Saxony-Anhalt (Landesverwaltungsamt Halle/S.).

Adult male Wistar rats (7–8 weeks old at the time of surgery) were used for the study. All efforts were made to minimize the number of rats used. After surgery, animals were housed individually, maintained on a 12 h light/12 h dark cycle, and had *ad libitum* access to water and food.

### Surgery

All rats underwent chronic implantation of electrodes in the OB and aPC (Supplementary Fig. 1A) as described previously (Strauch and Manahan-Vaughan 2018). For electrophysiological experiments conducted in the absence of fMRI, electrodes were made from polyurethane-coated stainless-steel wire (diameter: 127  $\mu\text{m}$ , Biomedical Instruments, Zöllnitz, Germany). Screws connected to silver-coated copper wire were used as ground and reference electrodes. For electrophysiology during fMRI experiments, recording and stimulating electrodes were made from Teflon-coated wolfram wire (diameter: 114  $\mu\text{m}$ ). Silver wires served as ground and reference electrodes, and plastic screws were used to stabilize the whole assembly. All rats were implanted under sodium pentobarbital anesthesia (Nembutal, 52 mg/kg; Narcoren, Boehringer Ingelheim Vetmedica GmbH, Ingelheim/Rhein, Germany). A monopolar recording electrode was placed in the lower layer I of the aPC (+3.2 mm anterior to bregma, 3.3 mm lateral from midline) and a bipolar stimulation electrode was positioned in the OB (+7.9 mm anterior to bregma, 1.1 mm lateral from midline). After the final evoked response remained stable, the electrode assembly was sealed and fixed to the skull with dental acrylic (Paladur, Heraeus Kulzer GmbH, Hanau, Germany). Pre- and postsurgery analgesia was implemented using Meloxicam subcutaneously (s.c., 0.2 mg/kg; Metacam, Boehringer Ingelheim Vetmedica GmbH, Ingelheim/Rhein, Germany).

Seven to ten days after surgery, the first experiments were conducted. During experiments, field excitatory postsynaptic potentials (fEPSPs) in the aPC were evoked by applying test-pulse stimulation or electrical patterned stimulation in the OB.

### aPC Responses during and after Electrical OB Stimulation

Electrophysiological responses in the aPC were evoked by test pulses applied at a low frequency (one pulse every 60 s) with single biphasic square wave pulses (0.2 ms duration per half wave) by stimulating the OB as described before (Strauch and Manahan-Vaughan 2018). The fEPSP was measured as the maximum slope from the onset of the fEPSP to the trough of the first negative deflection of the evoked response. First, one control experiment was performed to examine the stability of the

evoked response in behaving animals (Fig. 1A), and then all other experiments were performed (Fig. 1A,B).

#### Behaving Rats

During the first control experiment (Fig. 1A) that served to verify that the rats responded to OB stimulation, animals could move freely within the recording chamber ( $40 \times 40 \times 50$  cm) and disturbances of the animals were kept to an absolute minimum. The maximum fEPSP response was determined by means of an input/output (I/O) curve: Stimuli in the range of 100 to 900  $\mu$ A were applied in 100  $\mu$ A steps at 5 min intervals (three evoked responses were averaged per stimulus intensity). A stimulus intensity that produced 40–50% of the maximum response, determined by the I/O curve, was used to evoke responses during the remainder of the experiments. Here, five evoked responses were averaged for each time-point. The first six time-points recorded at 5 min intervals served as reference and all data points were calculated as a percentage of the mean of these first six time-points. After three more time-points were recorded at 5 min intervals, the interval between recordings was extended to 15 min, whereupon 15 time-points were subsequently recorded. On the morning following the experiment, another hour of recordings was conducted. Only rats exhibiting a stable recording during this first control experiment (Fig. 1A, [Supplementary Fig. 2](#)) were used for further experiments in the awake or sedated state (Fig. 1A,B).

In further experiments in awake, behaving animals, two different patterned afferent stimulation protocols were tested (100 and 20 Hz). Patterned afferent stimulation was applied after recording the first six reference time-points (Fig. 1A). Both stimulation protocols consisted of 20 trains, with each train being applied for 5 s with an interval of 55 s between trains. The pattern and frequency of the trains differed between the protocols (Fig. 1C). For the 100 Hz high-frequency stimulation (HFS) protocol, each train consisted of five bursts given at a frequency of 1 Hz. Each burst, in turn, contained 20 pulses applied at 100 Hz. This protocol is similar to protocols tested before in fMRI experiments examining the perforant path—dentate gyrus pathway (Angenstein et al. 2007, 2009, 2010). For the 20 Hz stimulation protocol, each train consisted of 100 consecutive pulses applied at 20 Hz. We chose the frequency of the second protocol to be in the range of beta oscillations (15–40 Hz), which are critically involved in olfactory information processing and memory (Kay et al. 1996; Ravel et al. 2003; Martin et al. 2004, 2006; Martin and Ravel 2014).

#### Sedated Rats

Experiments under medetomidine sedation (Fig. 1B) were performed in the same recording chamber as described for behaving rats so that animals could move freely after waking up. The experimental procedure was shortened compared with experiments in behaving animals to keep the time under sedation as short as possible. First, animals were anesthetized with isoflurane, a bolus of medetomidine (0.05 mg/kg; s.c.) was applied, and ca. 10 min later infusion of medetomidine (s.c.; 0.1 mg/kg per h) was started. Twenty to thirty min after bolus injection, a shortened I/O curve was recorded (100–700  $\mu$ A in 200  $\mu$ A steps). The first four time-points recorded at 5 min intervals served as reference for the calculation of the percentage of all time-points. The same electrical stimulation protocol (100 Hz; Fig. 1C), as used in the behaving animals, was applied afterwards, followed by recording of six more

time-points at 5 min intervals. Before the recording interval was extended to 15 min, sedated animals were treated with atipamezole (s.c., 0.1 mg/kg, Antisedan, Elanco Germany GmbH, Bad Homburg, Germany) as an antidote and then six more time-points were recorded in the now awake animals. A separate set of experiments was conducted without application of electrical stimulation (Fig. 1B). Here, instead of the stimulation protocol test-pulses were applied during a similar total duration of sedation as described above. These experiments were performed to control the stability of responses evoked by test pulses under sedation and to examine effects, on basal responses, of antidote treatment. One animal showed movements during these experiments; therefore, it was excluded from further analysis in the sedated group. In another animal, the evoked OB-aPC response was lost before the experiments under sedation, so that the total number of data sets analyzed was smaller ( $n = 7$ ) in the sedated groups (Fig. 1).

#### Electrical OB Stimulation during Functional Magnetic Resonance Imaging

All animals ( $n = 9$ ) were tested in two separate fMRI experiments, separated by an interval of at least 1 week. Two different patterns of 20 trains (55 s intertrain intervals) with each consisting of 100 pulses (applied within 5 s) were tested at a stimulation intensity of 400  $\mu$ A. Both protocols were the same as the ones used in electrophysiological experiments in the absence of fMRI (100 Hz protocol and 20 Hz protocol). To rule out that the stimulation protocol applied first has a subsequent impact on the second protocol, we randomized the order in which the animals were tested with the two stimulation protocols. Thus, in some of the animals, the 100 Hz protocol was tested first and 1 week later the 20 Hz protocol was tested. For the other animals, the stimulation protocols were tested in the opposite order.

#### Functional MRI (fMRI)

The procedure for MRI imaging with electrical stimulation followed established methods (Angenstein et al. 2007, 2009). All fMRI measurements were performed on a 4.7T Bruker Biospec 47/20 animal scanner (free bore of 20 cm) equipped with BGA09 (400 mT/m) gradient system (Bruker BioSpin GmbH, Ettlingen, Germany). For the radio frequency (RF) signal reception, a 50 mm “litzcage” small animal coil (Doty Scientific Inc.) was used. This is a circularly polarized form of volume coil that incorporates paralleled conductor elements with integrated crossovers, akin to linear litz coils, and capacitively segmented phase shifts that are a feature of small animal MRI birdcages (Doty et al. 2007). The litzcage coil is characterized by a high homogeneity; thus, no centering of the coil was necessary to maximize contrast-to-noise ratio.

Animals were initially anesthetized with isoflurane (1.5–1.8%; in 50:50 N<sub>2</sub>:O<sub>2</sub>; v:v), and the anesthesia was switched to deep sedation by application of medetomidine (Dorbene, Pfizer GmbH; bolus: 50  $\mu$ g/kg s.c. and after 15 min 100  $\mu$ g/kg per h s.c.) after animals were fixed into the head holder and connected to recording and stimulation electrodes. Breathing, heart rate, and oxygen saturation were monitored throughout the experiment by an MRI-compatible pulse oximeter (MouseOX; Starr Life Sciences Corp.) and heating was provided from the ventral site.

For anatomical images, 10 horizontal T<sub>2</sub>-weighted spin-echo images were obtained with a rapid acquisition relaxation enhanced (RARE) sequence (Hennig et al. 1986) with the following parameters: TR 4000 ms, TE 15 ms, slice thickness

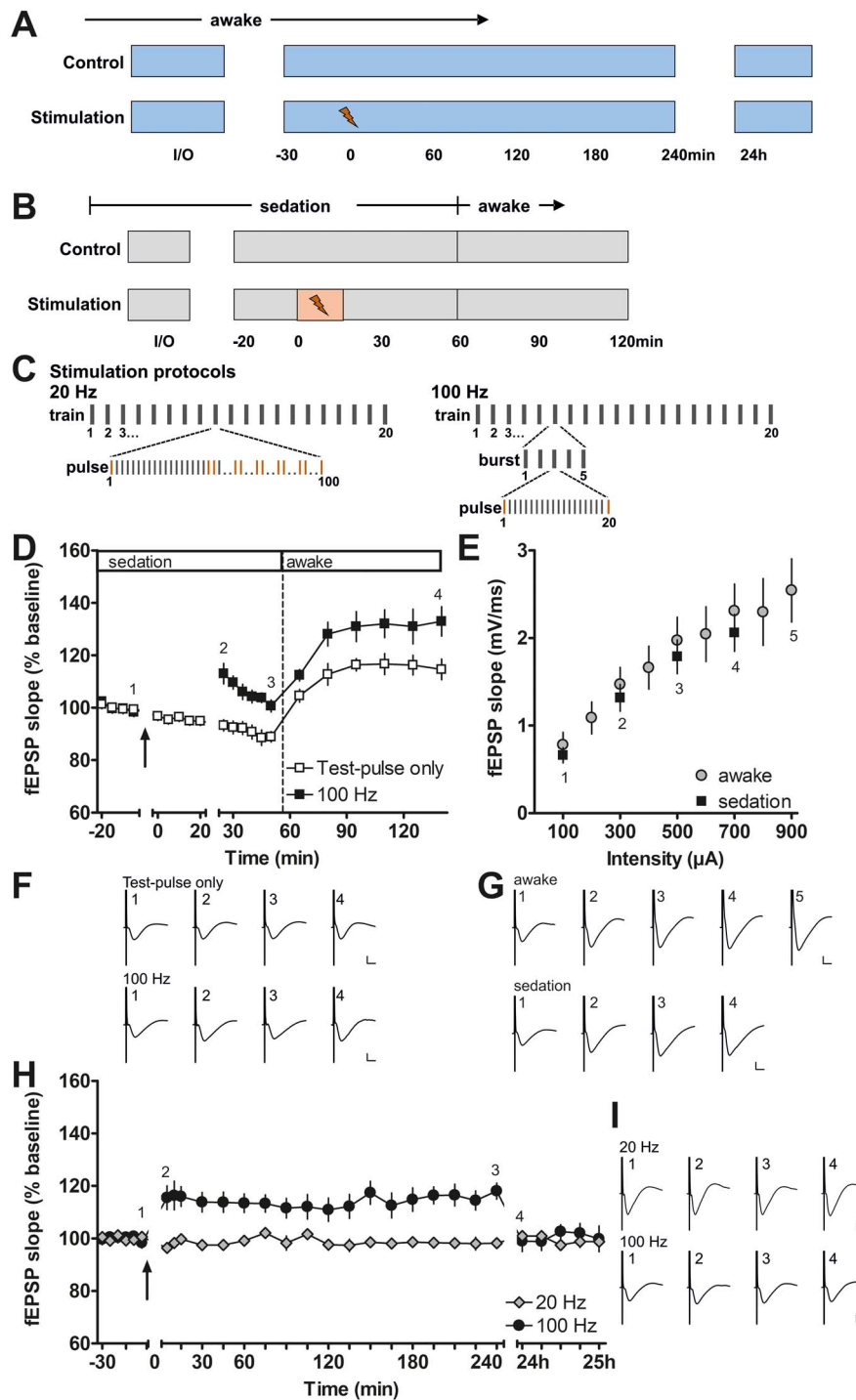


**Figure 1.** Long-term potentiation in the piriform cortex induced by prolonged electrical stimulation of the olfactory bulb in sedated and awake behaving rats. (A) Experimental procedure for testing prolonged patterned stimulation of the olfactory bulb, while recording in the anterior piriform cortex in awake behaving animals. During the control experiment, the stability of the evoked responses was confirmed. Only animals exhibiting stable evoked responses over the 25 h monitoring period were tested with prolonged patterned stimulation (20 and 100 Hz protocols). (B) Experimental procedure during fMRI-like conditions under medetomidine sedation. The total duration of medetomidine sedation was similar during control and stimulation (100 Hz protocol) experiments. (C) Scheme depicting the patterns of the 20 Hz (left) and 100 Hz (right) stimulation protocols. Both protocols consist of 20 trains with 100 pulses applied during each train. In the 20 Hz protocol, the 100 pulses of each train are applied consecutively at 20 Hz. Ten evoked responses to pulses 1, 20, 21, 40, 41, 60, 61, 80, 81, and 100 (marked in orange) were analyzed for each train during 20 Hz stimulation in behaving rats. In the 100 Hz protocol, each train contains five bursts and each burst contains 20 pulses applied at 100 Hz. For the analysis during 100 Hz stimulation, the responses (marked in orange) evoked by the 1st and 20th pulse of each burst were analyzed. (D, F) Patterned stimulation of the olfactory bulb at 100 Hz applied under medetomidine sedation ( $n = 7$ , black squares) induces long-term potentiation (LTP) lasting at least 2 h in the anterior piriform cortex. (Arrow indicates the start of 100 Hz stimulation). Where only test pulses were applied to the olfactory bulb (white squares), evoked potentials recorded in the piriform cortex decrease in magnitude during sedation and increase after the animals are awake. (F) Representative evoked responses recorded (1) 5 min before, (2) 5 min after, (3)

0.8 mm, FOV 37 × 37 mm, matrix 256 × 256, RARE factor 8, number of averages four. The total scanning time was 8 min 32 s.

fMRI was performed with a gradient EPI (echo planar imaging) sequence with the following parameters: TR 2000 ms, TE 24 ms, slice thickness 0.8 mm, FOV 37 × 37 mm, matrix 92 × 92, total scanning time per frame 2 s. The geometry used for anatomical images and functional images was identical, except the matrix that was 256 × 256 for anatomical and 92 × 92 for functional images. After an initial period of 2 min, electrical stimulation was applied every minute for 5 s, and thus, the total time for 20 stimulation trains was 22 min (corresponds to 660 frames). We did not use an EPI distortion correction algorithm because the distortions were slightly different in each individual measurement. For this reason, we choose to identify only major (significant) effects in the absence of EPI distortion correction. Although an EPI distortion correction algorithm would have allowed us to detect even larger activated regions than those that were found, we used the more conservative approach to be certain of the specificity of effects.

BOLD responses in the OB could not be analyzed due to its location at the anterior part of our region of interest. Responses in this area are subjected to a much stronger influence of artifacts, as can be seen in the examples of T2\*-EPI images (Supplementary Fig. 1B).

We recorded evoked potentials in the aPC during fMRI, but due to the small size of evoked responses that were disturbed by 50 Hz noise and occasionally by gradient artifacts, these could not be analyzed consistently (Supplementary Fig. 1C,D). Thus, the fEPSP responses evoked by patterned stimulation with the 100 Hz protocol were assessed in medetomidine sedated rats, whereas fEPSP responses evoked by both protocols were assessed in awake behaving rats.

### Temporally Compartmentalized Fluorescence In Situ Hybridization

Homer1a mRNA expression in the piriform cortex has been demonstrated to significantly increase after substance-induced, or electrically induced status epilepticus, as well as after sleep deprivation (Potschka et al. 2002; Cavarsan et al. 2012; Zhu et al. 2020). An increase in Homer1a mRNA expression in cell nuclei is detectable in the hippocampus and cortex ca. 25–40 min after the start of maximal electroconvulsive shock treatment, or after the start of spatial learning (Bottai et al. 2002; Vazdarjanova et al. 2002; Hoang et al. 2018, 2021). We used somatically expressed Homer1a mRNA as biomarker for somatic activation induced by HFS of the OB.

All animals were handled and evoked responses were tested on several days before the test day. On the test day, animals were habituated to the chamber and the I/O relationship (in 100  $\mu$ A steps ranging from 100 to 900  $\mu$ A) was recorded to determine the stimulus intensity for each animal that evokes 40–50% of the

maximum evoked response in the aPC. This stimulus intensity was then used for HFS in test animals and test-pulse stimulation in control animals. Test animals received HFS (100 Hz protocol) and control animals received test-pulse stimulation (1 pulse every 60 s) of the OB both lasting for 20 min. Brains of test and control animals were removed quickly 35–40 min after the start of HFS or test-pulse stimulation. For the aPC analysis, we added an additional naive (unstimulated) group to clarify whether OB stimulation changes Homer1a expression. The naive animals were handled and habituated to the chamber on several consecutive days for at least 1 h per day. On the test day, brains were quickly removed after the habituation period.

After removal, each brain was quickly shock-frozen in 2-methyl butane held in a metal container surrounded by liquid nitrogen. Coronal sections (20  $\mu$ m thick) were cut on a cryostat (Leica CM 3050S) and mounted on glass slides (SuperFrost Plus, Gerhard Menzel GmbH). For further processing, slides containing either the AON (ca. +5.0 mm to +5.5 mm anterior to bregma) or the prelimbic–infralimbic cortex (PrL-IL) and aPC (ca. +3.0 to +3.5 mm anterior to Bregma) were chosen according to a rat brain atlas (Paxinos and Watson 2014).

Homer1a cDNA plasmids were prepared by Genscript Biotech using a 1.2 kb Homer1a transcript according to the sequence (Genebank U92079\_1) of Brakeman et al. (1997). The plasmids were linearized (NewEngland Biolabs GmbH) and purified with QIAprep Miniprep Kit (#27104; Qiagen N.V.). Homer1a cRNA probes were generated using an in vitro transcription kit (MaxiScript Kit T7; Invitrogen) and premixed RNA labeling nucleotides containing Digoxigenin-11-UTP (#10451422; Roche Diagnostics). Yield and integrity of the purified RNA probes were verified using gel electrophoresis, and the concentration was measured using Quantus Fluorometer (Promega).

Fluorescence in situ hybridization for digoxigenin-labeled probes was adapted from Guzowski and Worley (2001) and performed in a similar manner as described previously (Sethumadhavan et al. 2020). To confirm the specificity of the labeling for each staining procedure, one slide per sample set served as a negative control and underwent all staining procedures except for the addition of RNA. Slides were fixed in polyoxymethylene in phosphate-buffered saline (PBS), washed in 2-fold concentrated saline-sodium citrate (SSC), and left in acetic anhydride solution. Then, they were washed in 2-fold concentrated (2 $\times$ ) SSC. Slides were incubated at 37 °C in prehybridization buffer (1:1; 4 $\times$  SSC: formamide) for 10 min and rinsed afterwards in 2 $\times$  SSC. A humidity chamber was prepared with soaked filter paper (1:1; 2 $\times$  SSC: 50% deionized formamide). The digoxigenin-labeled RNA probe was diluted in 1 $\times$  hybridization buffer (1 ng/1  $\mu$ L; Sigma-Aldrich), heated to 90 °C, and distributed on each slide. Then slides were covered with laboratory film (Parafilm, Bemis) and cover glass, and afterwards hybridized for ca. 17 h in the humidity chamber at 56 °C. The following stringent washing steps were then conducted: Slides were washed in 2 $\times$  SSC at 56 °C and left

30 min after, and (4) 2 h after the end of patterned stimulation. (E, G) Comparison of input–output relationship for fEPSP responses recorded in the piriform cortex of sedated ( $n = 7$ ) and awake ( $n = 9$ ) rats evoked by test pulses applied to the olfactory bulb. All values shown in these graphs were recorded at the start of the experiments where the 100 Hz protocol was applied. (G) Representative evoked responses recorded during the evaluation of the input–output relationship at a stimulus intensity of (1) 100  $\mu$ A, (2) 300  $\mu$ A, (3) 500  $\mu$ A, (4) 700  $\mu$ A, and additionally in awake animals (5) 900  $\mu$ A. (H, I) Patterned stimulation at 100 Hz, applied to the olfactory bulb in awake behaving rats ( $n = 9$ ), induces LTP lasting for at least 4 h in the anterior piriform cortex. In contrast, 20 Hz stimulation ( $n = 8$ ) does not change synaptic strength. Arrow indicates application time of patterned stimulation at 20 Hz, or 100 Hz. Graphs comparing 20 and 100 Hz stimulation to test-pulse stimulation are provided in Supplementary Fig. 2. (I) Representative evoked responses recorded (1) 5 min before, (2) 5 min after, (3) 4 h after, and (4) 24 h after patterned stimulation. F, G, I calibration: vertical bar: 1 mV, horizontal bar: 5 ms. D, E, H mean  $\pm$  SEM.

in RNase A (Merck KGaA, Darmstadt, Germany) in  $2\times$  SSC. Subsequently, slides were washed in  $2\times$  SSC at  $37^\circ\text{C}$ ,  $0.5\times$  SSC at  $56^\circ\text{C}$ ,  $0.5\times$  SSC at  $56^\circ\text{C}$ ,  $0.5\times$  SSC at room temperature (RT),  $1\times$  SSC at RT, and rinsed in Tris-buffered saline (TBS) at RT. Signals were detected using immunohistochemistry. After  $\text{H}_2\text{O}_2$  pretreatment and blocking, Homer1a-digoxigenin was detected by anti-digoxigenin-peroxidase (1:2000; Roche Holding AG) in  $1\times$  animal-free blocker (Vector Labs) and TBS-Tween (Sigma-Aldrich). Then slides were rinsed and the signals were enhanced using biotinylated tyramine (Adams 1992). After rinsing, Homer1a mRNA was detected using Streptavidin Cy5 (Dianova GmbH). Slides were rinsed, washed in distilled water, dipped in 70% ethanol, and stained using 1% Sudan black B (Merck KGaA) in 70% ethanol (Oliveira et al. 2010). Then they were washed in distilled water and air-dried overnight. Nuclei were visualized using 4',6-diamidino-2-phenylindole (DAPI) in mounting medium (SCR-038448, Dianova GmbH).

### Verification of Electrode Positions

In fMRI experiments, anatomical scans were examined to identify the location of the stimulation electrode in the OB (Supplementary Fig. 1A). For the other experiments, brains were removed at the end of the study for histological verification of the electrode position in the OB and aPC. Sections were stained in 0.1% cresyl violet following a procedure described previously (Hansen and Manahan-Vaughan 2015). Animals with incorrectly implanted electrodes were excluded from further analysis.

### Data Processing and Analysis

#### Electrophysiology

All data from electrophysiological experiments were expressed as a mean percentage  $\pm$ SEM of the average reference value and were visualized using GraphPad Prism software (GraphPad Software, Inc.). For analysis of the evoked responses during HFS (Fig. 2, Supplementary Fig. 3), the fEPSP slopes of the first and the 20th response of each burst of each train were calculated. For 20 Hz stimulation the fEPSP slopes of 10 pulses of each train were obtained (Supplementary Fig. 3). All absolute values  $\pm$ SEM were then determined. Using Statistica software (StatSoft, Inc.), analysis of variance with repeated measures (rmANOVA) was conducted to analyze differences between patterned stimulation and test-pulse stimulation. To examine changes in evoked responses during prolonged electrical stimulation, one-way ANOVA was performed for fEPSP slopes of the sedated group. In the awake group, 10 evoked responses of the 100 Hz protocol could not be analyzed due to movements affecting the recordings. In three of the rats, only intermittent data were obtained during application of the 100 Hz protocol in the electrophysiological experiments. For this reason, these rats were not included in the statistical analysis of electrophysiological responses. For 20 Hz stimulation, one animal was excluded from the analysis during application of the stimulation protocol due to problems with the recorded signals. The level of significance was set to  $P < 0.05$  and  $n$  corresponds to the number of animals.

#### Functional Magnetic Resonance Imaging Data

The fMRI data were converted to BrainVoyager data format. A standard sequence of preprocessing steps was applied to each data set by means of BrainVoyager QX 2.8.0 software (Brain Innovation), including slice scan time correction, 3D motion

correction (trilinear interpolation and reduced data using the first volume as a reference), and temporal filtering (FWHM 3 data points). Because the reconstruction of the fMRI images resulted in a  $128\times 128$  matrix (instead of a  $92\times 92$  imaging matrix), spatial smoothing (Gaussian filter of 1.4 voxel) was applied.

**General linear model analysis.** Each individual functional data set was used for multiple-subject general linear model (GLM) analysis implemented in BrainVoyager QX 2.8.0 software. Functional activation was analyzed by using the correlation of the observed BOLD signal intensity changes in each voxel with a predictor (hemodynamic response function) generated from the respective stimulus protocol (see above). Based on this, the appropriate 3D activation map could be generated. To calculate the predictor, the square wave representing stimulus-on and stimulus-off conditions was convolved with a double gamma hemodynamic response function (onset 0 s, time to response peak 5 s, time to undershoot peak 15 s). To exclude false-positive voxels, a correction for serial correlation (csc) was performed (implemented in the BrainVoyager QX 2.8.0 software), and we considered only those with a significance level ( $P$ ) above the threshold set by calculating the false discovery rate (FDR) with a  $q$ -value of 0.001 (which corresponds to a  $t$ -value greater than 4.29 or  $P < 1.8\times 10^{-5}$ ).

**Second-level group analysis.** To visualize significant differences in BOLD responses between the two stimulation conditions, a fixed-effect analysis with a GLM, including  $z$ -transformed functional data of all animals, was performed using the 2-gamma response function implemented in BrainVoyagerQX. All significantly activated voxels (threshold FDR  $q$ -value of 0.05, Bonferroni correction) were converted into volumes of interest (VOI), from which surface clusters were created and visualized with the BrainVoyager VOI analysis tool.

**VOI analysis.** Each individual functional imaging data set was aligned to a 3D standard rat brain using the 3D volume tool implemented in BrainVoyager QX 2.8.0 software. Using established methods (Bovet-Carmona et al. 2019; Helbing and Angenstein 2020), the following VOIs were marked individually in a 3D standard rat brain that was generated from a rat of the same age and strain: right/left hippocampus (HC), right/left entorhinal cortex (EC), right/left nucleus accumbens, right/left striatum, right/left basolateral amygdala (BLA), right/left piriform cortex, right/left AON, dorsal medial prefrontal cortex (mPFC), PrL-IL, nucleus of the vertical limb of the diagonal band (VDB), septum, and ventral tegmental area-substantia nigra (VTA-SN). With regard to the VOIs located more medially in the brain, the spatial resolution of fMRI recordings did not permit an unambiguous distinction of left and right hemispheres. Thus, for analysis, each was considered as a single midline structure. The averaged BOLD time series of all voxels located in one VOI was calculated for each individual animal using the volume-of-interest analysis tool implemented in the BrainVoyager QX 2.8.0 software. Each individual BOLD time series was normalized using the averaged BOLD signal intensity of 100%. All normalized BOLD time series were averaged and depicted as mean BOLD time series  $\pm$ SD. Based on the calculated BOLD time series, event-related BOLD responses were calculated by measuring the signal intensities starting six frames before stimulus onset ( $-12$  s until 0 s), during stimulus presentation (between 0 s and 4 s, which corresponds to two frames), and the following 15 frames (8–38 s) after the end of the stimulus. To avoid the confounding effect of putative variations in baseline BOLD signal intensities on the calculated BOLD response (i.e.,  $\text{BOLD signal}_{\text{stimulus}}/\text{BOLD}$

signal<sub>baseline</sub> \* 100%), each BOLD response was related to BOLD signal intensities of the stimulus over the preceding 12 s.

#### Fluorescence In Situ Hybridization Data

Nuclear Homer1a mRNA expression was examined in sections of the left (unstimulated) and right (stimulated) hemispheres of control (test-pulse stimulation;  $n=7$ ) and test (100 Hz;  $n=6$ ) animals for the following regions: dorsal part of the anterior olfactory nucleus (AOD), lateral part of the anterior olfactory nucleus (AOL), infralimbic (IL) and prelimbic cortex (PrL), and lower layer 2 of the anterior piriform cortex (aPC). With regard to the left and right aPC, an additional naïve (nonstimulated) group ( $n=6$ ) was additionally analyzed. Images of slices containing the regions of interest (ROIs) were obtained using a slide scanner microscope (20× magnification; AxioScan.Z1, Zeiss). For each region, ROIs were defined in the left and right hemispheres in three slices of an animal. Thus, three ROIs were analyzed for each animal of a group. DAPI-stained nuclei were identified using ImageJ software (Schindelin et al. 2012). Nuclei containing Homer1a mRNA were counted during experimenter-blind analysis. The percentage of Homer1a-positive nuclei was calculated from all nuclei of each ROI. The mean percentage of positive nuclei of three ROIs was calculated for each region of each animal. The mean percentage  $\pm$ SEM of positive Homer1a nuclei was calculated for all animals of a group. In one control animal, AOD and AOL could not be analyzed, because these sections were not collected during cutting; thus, animal numbers are smaller for these regions (control and 100 Hz,  $n=6$ , each). The results were examined for outliers and normal distribution (Kolmogorov-Smirnov test). Two outliers, one in the AOD and one in the AOL, tested with the extreme studentized deviate (ESD) method, were removed from the control group of the right hemisphere (indicated in [Supplementary Fig. 4](#)). For subsequent statistical analysis of each region, a multifactorial ANOVA with subsequent post hoc analysis (Fisher's LSD test) was performed. Hemisphere (left; right) and treatment (control; 100 Hz; naïve only for aPC) were used as factors. The level of significance was set to  $P < 0.05$  and  $n$  corresponds to the number of animals.

## Results

### Patterned Stimulation of the Olfactory Bulb at 100 Hz Triggers LTP in the Anterior Piriform Cortex

To induce LTP in the aPC, the OB received HFS at 100 Hz. In medetomidine-treated animals ( $n=7$ ), this resulted in a significant potentiation of evoked responses (Fig. 1D,F) compared with medetomidine-treated animals serving as control-stimulated controls ( $n=7$ ) (rmANOVA:  $F_{1,12} = 20.526$ ,  $P < 0.001$ ). Recordings were obtained for 60 min, after which time the animals were roused from sedation, at which point an increase in the magnitude of evoked responses was detected in both control and test animals. The potentiation was nonetheless sustained in HFS-stimulated animals compared with control animals (rmANOVA:  $F_{1,12} = 6.991$ ,  $P < 0.05$ ). Overall, a significant potentiation was evident throughout the entire post-HFS recording period in animals that received HFS (rmANOVA:  $F_{1,12} = 13.080$ ,  $P < 0.01$ ).

To assess the stability and persistency of LTP induced by HFS at 100 Hz of the OB, we repeated the experiment in freely behaving rats (Fig. 1, [Supplementary Fig. 2A](#)). In addition, we assessed the effect of 20 Hz stimulation containing the same total number of pulses (Fig. 1, [Supplementary Fig. 2B](#)). Both protocols were later tested and compared during fMRI recordings.

The I/O relationship of sedated and awake rats was similar (Fig. 1E,G; sedation:  $n=7$ , awake:  $n=9$ ) suggesting that medetomidine had only minor effects on synaptic transmission in the aPC during the initial phase of sedation.

In awake animals, HFS at 100 Hz resulted in stable LTP (rmANOVA:  $F_{1,16} = 8.665$ ,  $P < 0.01$ ) that persisted for at least 4 h but had declined to baseline values by 24 h post-HFS (post hoc Fisher's LSD), compared with control animals that received test pulses only ( $n=9$ , each). In contrast, the 20 Hz protocol did not affect synaptic transmission in comparison to test-pulse stimulation ( $n=8$ , each; rmANOVA:  $F_{1,14} = 0.05$ ,  $P = 0.824282$ ). A comparison of the effects of both stimulation protocols on evoked responses in the aPC revealed that they are significantly different (rmANOVA:  $F_{1,15} = 10.678$ ,  $P < 0.01$ ).

### Synaptic Transmission in the Anterior Piriform Cortex Changes Dramatically during HFS at 100 Hz of the Olfactory Bulb

To elucidate the immediate impact of HFS on the evoked responses in the aPC, we examined how evoked responses change over the course of patterned stimulation of the OB with both the patterned stimulation protocols. Therefore, in the 100 Hz protocol, we analyzed two evoked responses (1st and 20th) in each burst of each train (Fig. 1C). For the 20 Hz protocol, we analyzed 10 pulses of each train (Fig. 1C). Thus, for both protocols we analyzed a total of 200 of all 2000 evoked responses in all 20 trains (Fig. 2, [Supplementary Fig. 3](#)). Under medetomidine sedation, fEPSPs changed significantly over the course of patterned stimulation at 100 Hz ( $n=7$ ; one-way ANOVA:  $F_{199,1200} = 12.72$ ,  $P < 0.0001$ ). In awake animals, fEPSPs evoked with 100 Hz stimulation changed in a similar manner over time ([Supplementary Fig. 3A-C](#);  $n=6$ ; one-way ANOVA:  $F_{199,990} = 2.125$ ,  $P < 0.0001$ ). In contrast to patterned stimulation at 100 Hz, during 20 Hz stimulation ([Supplementary Fig. 3D,E](#)), no significant change was detected over the course of stimulation ( $n=7$ ; one-way ANOVA:  $F_{199,1200} = 0.218$ ,  $P = 1.000$ ) in behaving rats. For the 100 Hz protocol, in particular under sedation, it was apparent that the first evoked responses of this protocol were larger than the 20th evoked responses for every burst and every train (Fig. 2A-C). These short-term depression effects during each burst of stimulation are likely the result of less neurotransmitter being released presynaptically during the course of each burst (Zucker and Regehr 2002).

### Patterned Stimulation of the Olfactory Bulb Changes BOLD Response in Olfactory Cortex Regions

Having observed that OB-aPC synapses respond to 100 Hz stimulation with LTP, we used fMRI imaging ( $n=9$ ), to examine if BOLD responses are changed over the time course of patterned stimulation (Fig. 3). We compared BOLD responses to 100 Hz (that induces aPC-LTP) and to 20 Hz stimulation (that has no effect on evoked responses in the aPC). Volume of interest (VOI) analysis revealed that over the time course of patterned stimulation both protocols induce pronounced changes in BOLD signals in several of the analyzed brain regions (Fig. 3).

For olfactory cortex regions, BOLD signals changed in the anterior olfactory nucleus (AON) and piriform cortex (Figs 3 and 4). A higher amount of significant change in BOLD signals was detected in the right (stimulated) hemisphere compared with the left (unstimulated) hemisphere (Fig. 3). For the right piriform cortex, 100 Hz stimulation of the OB resulted in significantly

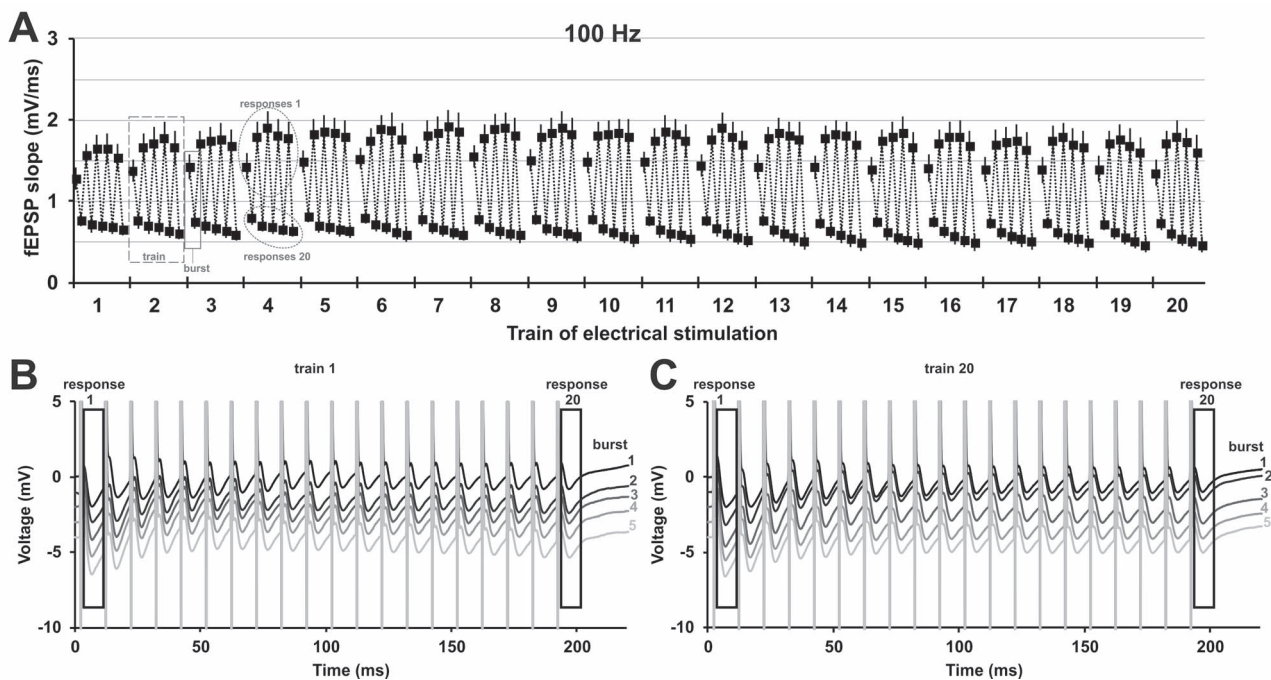


**Figure 2.** Patterned stimulation of the olfactory bulb changes synaptic responses in the anterior piriform cortex in a distinct manner. (A) Analysis of every 1st and 20th evoked response of each burst during patterned stimulation at 100 Hz ( $n = 7$ ) revealed that the fEPSP changes under medetomidine sedation (mean  $\pm$  SEM is shown). The 100 Hz stimulation consisted of 20 trains, each train contained five bursts, and every burst consisted of 20 pulses applied at 100 Hz (see Fig. 1C). Evoked responses of pulse 1 and pulse 20 of every burst are displayed (the two analyzed responses of burst 1 in train 3 are marked with a box with a solid line). Thus, for every train (train 2 is marked as example with a box with a dashed line), a total of 10 responses were analyzed (five 1st responses and five 20th responses, example in circle with dotted outline). (B, C) Representative examples of evoked responses of train 1 and train 20 recorded during prolonged patterned stimulation. Every 1st (response 1) and every 20th (response 20) evoked response of each burst was analyzed for (A) and are marked with an outline. The trace of each subsequent burst is plotted with an offset of  $-1$  mV to the previous burst. (B) Evoked responses of train 1 during each of the five bursts of patterned stimulation (burst 1–5: top to bottom, black to light gray). (C) Evoked responses of train 20 during each of five bursts of stimulation (burst 1–5: top to bottom, black to light gray).

stronger BOLD responses over the course of patterned stimulation, compared with 20 Hz stimulation, and, similarly, in the left piriform cortex, significant BOLD responses were only detectable during 100 Hz stimulation (Figs 3 and 4A–F).

By contrast, BOLD responses in the right AON were similarly elevated during the two stimulation conditions (Figs 3 and 4G–I). However, BOLD responses in the left AON were significantly stronger during 100 Hz stimulation, compared with 20 Hz stimulation (Figs 3 and 4J–L). A drift in BOLD baseline over the course of fMRI imaging was detected in the right AON for both stimulation protocols starting directly after the first train of stimulation (Figs 3 and 4G).

An elevation in the BOLD response was detected in the right entorhinal cortex during both 20 and 100 Hz HFS (Fig. 5). Using a second-level analysis to compare the difference between both stimulation protocols for only significantly activated voxels (GLM analysis) reveals that mainly the left AON and parts of the right piriform cortex were more strongly activated by the 100 Hz protocol compared with 20 Hz stimulation (Fig. 7), consistent with the results of the VOI analysis.

### BOLD Responses in Regions outside of the Olfactory Cortex Are Changed by Patterned Olfactory Bulb Stimulation

OB stimulation also triggered BOLD responses in structures that are not ostensibly part of the olfactory system (Figs 3, 5–7). We detected significant BOLD responses in the right nucleus

accumbens and the right basolateral amygdala (BLA; Figs 3 and 5), as well as the dorsal medial prefrontal cortex, the prelimbic-infralimbic cortex (PrL-IL), and the ventral diagonal band of Broca (VDB) (Figs 3 and 6). A significant shift in BOLD baseline of the BLA is detectable during the last trains of 100 Hz stimulation (Fig. 3). For the PrL-IL, 100 Hz stimulation was significantly more effective in changing BOLD signals compared with 20 Hz OB stimulation.

### An Increase in BOLD Response Induced by HFS Is Accompanied by a Change in Nuclear Expression of Immediate Early Gene mRNA in Olfactory and Prelimbic/Infralimbic Cortices

Homer1a mRNA expression can be used as a precise biomarker of neuronal activity (Brakeman et al. 1997). Both behavioral experience, or afferent stimulation results in a temporally confined increase in somatic Homer1a mRNA expression in the hippocampus and cortex that can be used as an accurate readout for experience-dependent information encoding (Vazdarjanova et al. 2002; Hoang et al. 2018; Strauch and Manahan-Vaughan 2020). Thus, using fluorescence in situ hybridization, we assessed if brain regions that exhibited higher changes in BOLD responses following 100 Hz OB stimulation (compared with 20 Hz stimulation) also exhibit somatic expression of the immediate early gene Homer1a, reflecting information encoding (Fig. 8, [Supplementary Figs 4–7](#)). We distinguished between unstimulated (left) and stimulated (right) hemispheres in the

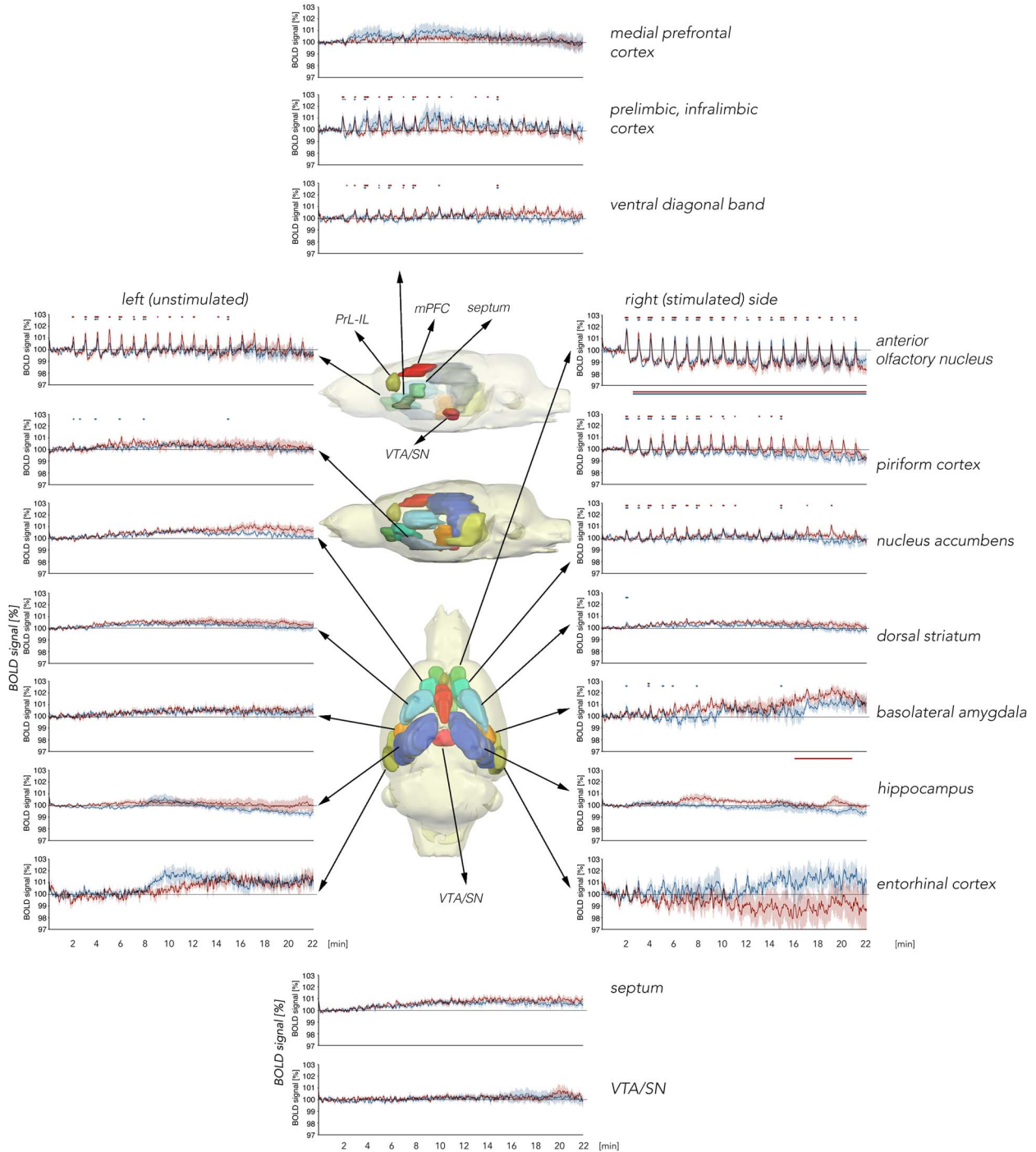


**Figure 3.** Summary of BOLD responses for VOI analysis over the course of patterned stimulation of the olfactory bulb. The brain schemata shown in the central section are lateral views from the left (unstimulated) hemisphere as well as a top view of a 3D standard rat brain containing all analyzed brain regions in different colors. The upper lateral brain diagram highlights all medial brain regions analyzed. The brain diagram below it shows a lateral view of other brain regions that were analyzed. These are also highlighted in the bottom “top view” brain diagram. The graphs represent volume of interest (VOI) analysis for BOLD time series in individual brain regions. BOLD time series for medial brain regions are shown in the graphs in the top and bottom central sections. Graphs depicting results from lateral brain regions are separated into right (stimulated) and left (unstimulated) hemispheres, for the recording time of 22 min during 20 trains of patterned stimulation at 100 Hz (red curves,  $n=9$ ) or at 20 Hz (blue curves,  $n=9$ ) of the olfactory bulb. Every significant change in BOLD signals is marked above each graph (red line: 100 Hz stimulation, blue line: 20 Hz stimulation). Significant BOLD responses from baseline are detectable in the anterior olfactory nucleus (AON), right/left piriform cortex, right nucleus accumbens, right basolateral amygdala, right dorsal striatum, the prelimbic–infralimbic cortex (PrL-IL), and ventral diagonal band of Broca. Significant shifts (decrease or increase) of baseline BOLD signals are marked below the graph (red line: 100 Hz stimulation; blue line: 20 Hz stimulation). A significant shift in baseline BOLD signals is visible for the right AON and right basolateral amygdala. VTA/SN: ventral tegmental area/substantia nigra, mPFC: dorsal medial prefrontal cortex. Mean BOLD time series  $\pm$ SD.

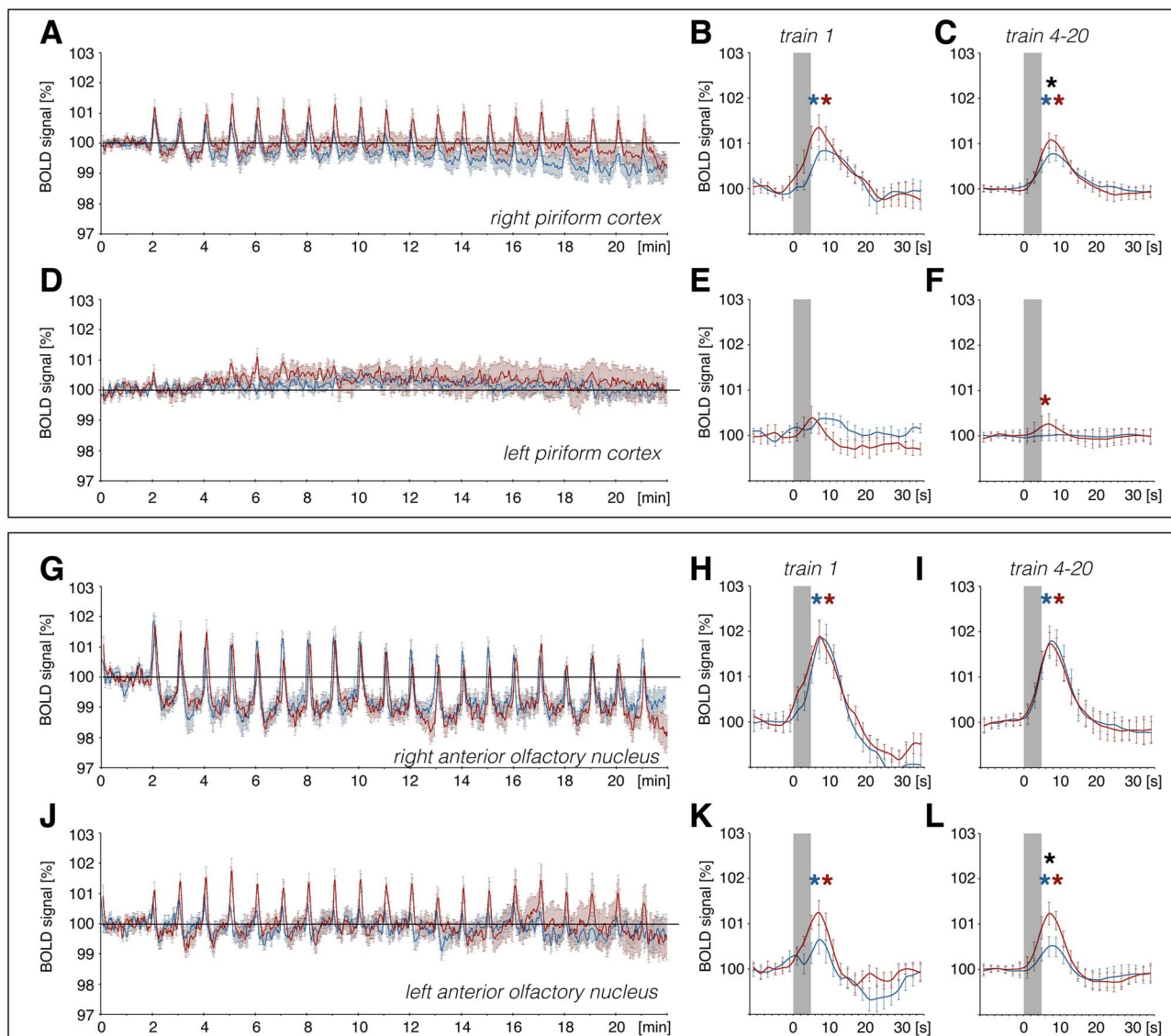


**Figure 4.** Patterned stimulation of the olfactory bulb induces a change in BOLD responses in the piriform cortex and anterior olfactory nucleus. VOI analysis of BOLD responses in the piriform cortex and anterior olfactory nucleus (AON) for the right (stimulated) and left (unstimulated) hemisphere during 100 Hz (red curve) and 20 Hz stimulation (blue curve) of the olfactory bulb (OB). (A, D, G, J): Enlarged image of piriform cortex and AON from Fig. 2. (A–F): BOLD time series of the (A) right and (D) left piriform cortex showing changes in BOLD signals over the time course of fMRI imaging. A significant BOLD response can be detected for train 1 and train 4–20 in the right piriform cortex and for trains 4–20 for 100 Hz stimulation in the left piriform cortex. No significant difference in evoked BOLD response between stimulation protocols can be detected for the first train (train 1) in the (B) right and (E) left piriform cortex. The mean of BOLD responses for trains 4–20 reveal a significantly stronger effect of 100 Hz stimulation on BOLD signals in the (C) right piriform cortex when compared with 20 Hz stimulation of the OB. (G–L): BOLD time series for the (G) right and (J) left AON depicting strong changes in BOLD responses as well as a decrease in baseline BOLD responses in the right AON. A significant BOLD response for both protocols (train 1 and trains 4–20) can be detected in the left and right AON. No significant difference in evoked BOLD response between stimulation protocols can be detected for train 1 in the (H) right and (K) left AON. For trains 4–20, mean BOLD responses in the (I) right AON do not differ between both stimulation protocols, whereas in the (L) left AON, trains 4–20 show a significant stronger BOLD response for 100 Hz stimulation compared with 20 Hz stimulation of the OB. Significant difference between stimulation protocols are marked with a black asterisk (\*), whereas significant BOLD responses induced by 100 Hz or 20 Hz stimulations are indicated with a red or blue asterisk, respectively. The gray box indicates the stimulation period.

following brain regions: aPC, dorsal part of the AON (AOD), lateral part of the AON (AOL), PrL, and IL.

As described above, the aPC expressed LTP in response to 100 Hz OB stimulation. With regard to nuclear Homer1a expression (Fig. 8C), a significant difference between the three groups (naïve:  $n = 6$ , control:  $n = 7$ , 100 Hz:  $n = 6$ ) was detectable (multifactorial ANOVA:  $F_{2,32} = 6.96286$ ,  $P < 0.01$ ). Naïve animals (no stimulation) expressed low levels of Homer1a mRNA in the nuclei of

the aPC: In the right (stimulated) hemisphere, a significant difference was visible for naïve, in comparison to 100 Hz stimulated (post hoc:  $P < 0.001$ ), and in comparison with test-pulse stimulated control animals (post hoc:  $P < 0.05$ ). This suggests that not only 100 Hz HFS but also test-pulse stimulation of the OB affects neuronal gene encoding in the stimulated hemisphere to a small extent. No changes in basal synaptic transmission were caused by test-pulse stimulation, indicating that the Homer1a mRNA

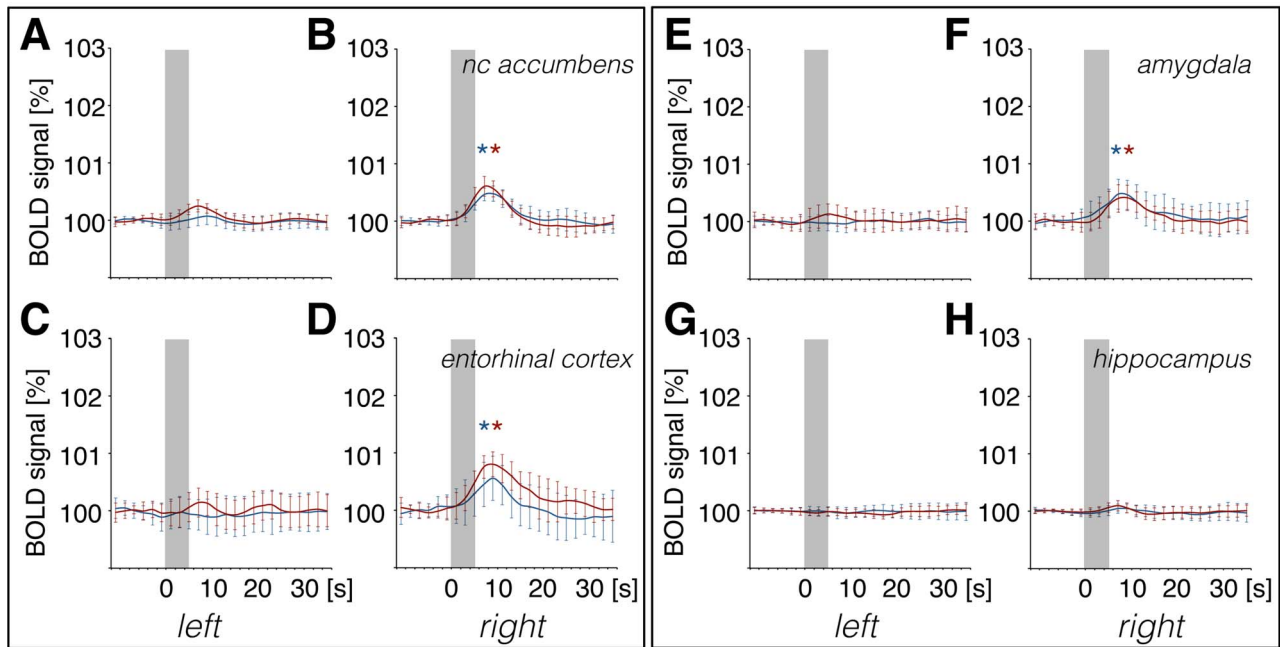


**Figure 5.** Patterned stimulation of the olfactory bulb results in strong changes in BOLD signals in brain regions of the right (stimulated) and less pronounced changes in the left hemisphere. Summary of mean ( $\pm$ SD) BOLD responses of trains 4–20 determined by volume of interest (VOI) analysis for patterned stimulation of the olfactory bulb at 100 Hz (red curve) and at 20 Hz (blue curve). A significant BOLD response was detected in (B), the right nucleus accumbens, (D), the right entorhinal cortex, and (F), the right basolateral amygdala. The corresponding left hemispheres of (A) the nucleus accumbens, (C) entorhinal cortex, and (E) amygdala were unaffected. No change in BOLD responses was detected in either the left (G) or right (H) hippocampus. BOLD responses for each train were normalized to exclude effects due to baseline shifts. Gray boxes indicate the stimulation periods. Significant BOLD responses induced by 100 Hz or 20 Hz are indicated with a red or blue asterisk, respectively.

increases detected in layer 2 of the aPC following test-pulse stimulation were not sufficient to induce significant changes in basal synaptic transmission recorded in layer 1 (Supplementary Fig. 2).

Consistent with the signal increases detected in the AON using BOLD fMRI, nuclear Homer1a mRNA expression was significantly increased in both the AOD (Fig. 8D) and the AOL (Fig. 8E) after 100 Hz stimulation ( $n=6$ ) compared with controls ( $n=5/6$  right/left hemisphere) (multifactorial ANOVA: AOD:  $F_{1,19} = 22.56057$ ,  $P < 0.001$ ; AOL:  $F_{1,19} = 14.85758$ ,  $P < 0.01$ ). For both areas of the AON, 100 Hz HFS significantly elevated Homer1a mRNA expression levels in the right (stimulated) hemisphere compared with test-pulse stimulated controls (left and right hemisphere) and the area of the left hemisphere after 100 Hz HFS (Fig. 8, see caption for all post hoc results).

Examination of Homer1a mRNA expression in PrL (Fig. 8F) in test-pulse stimulated controls ( $n=7$ ) and 100 Hz-stimulated animals ( $n=6$ ) revealed a significant increase in immediate early gene (IEG) expression induced by 100 Hz stimulation ( $F_{1,22} = 13.45290$ ,  $P < 0.01$ ) detectable in the unstimulated hemisphere (post hoc:  $P < 0.01$ ), whereas a trend toward an increase in IEG expression in the stimulated hemisphere was not significant. In the IL (Fig. 8G), 100 Hz stimulation of the OB resulted in a significant increase in somatic IEG expression (multifactorial ANOVA;  $F_{1,22} = 7.60369$ ,  $P < 0.05$ ) that is visible in the stimulated hemisphere compared with controls (post hoc:  $P < 0.05$ ).

These findings support that information encoding is triggered in olfactory cortex regions, and in the infralimbic and prelimbic cortices, following plasticity-related OB stimulation. The finding that the IL and PrL engage in gene

encoding in response to the activation of the OB is particularly striking.

## Discussion

In this study, we describe elements of an olfactory connectome that is activated when the OB drives information storage in the form of LTP in the aPC. Using fMRI, we identified subcortical and cortical brain regions that are activated during information transmission from the OB. In addition, using temporally compartmentalized fluorescence in situ hybridization we identified which of those regions engage in somatic gene encoding in response to OB-aPC information storage. Many of the structures that we identified as responders to OB information transmission have already been described as playing a role in odor processing, discrimination, and valence interpretation (anterior olfactory nucleus, piriform cortex, entorhinal cortex, basolateral amygdala, dorsal striatum, and nucleus accumbens). But the present study supports that the infralimbic and the prelimbic cortices also play a role in odor information encoding. Our study reveals an olfactory connectome that spans cortical and subcortical structures, which engages in odor processing and evaluation per se, of which only a select few members (PC, AON, PrL, and IL) engage in de facto information storage and/or encoding.

### Frequency-Dependent Induction of LTP in Olfactory Bulb–Anterior Piriform Cortex Synapses

HFS of the OB applied at 100 Hz, but not 20 Hz, resulted in LTP in the aPC. We previously reported that stimulation of the OB with

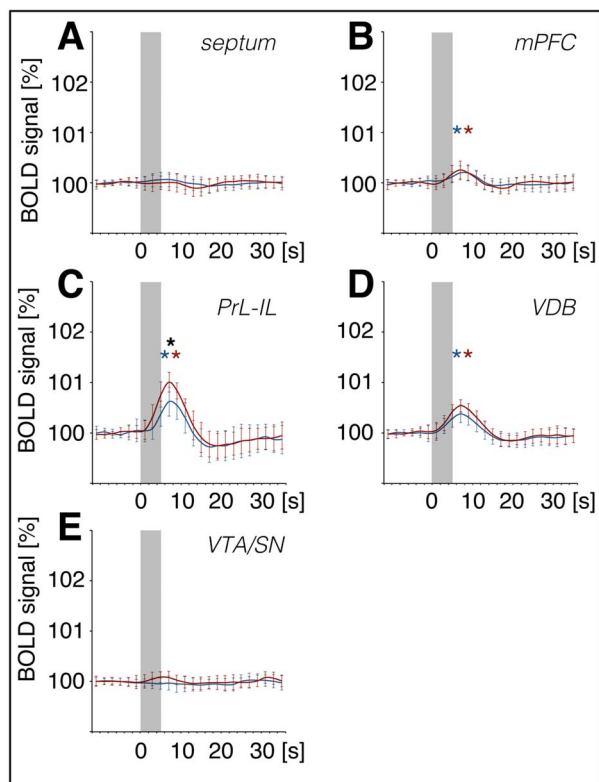


**Figure 6.** BOLD signals in the prelimbic–infralimbic cortex and ventral diagonal band of Broca increase during patterned stimulation of the olfactory bulb. Summary of mean ( $\pm$ SD) BOLD responses for trains 4–20, as determined by volume of interest (VOI) analysis for medial brain regions: (A) Septum, (B) dorsal medial prefrontal cortex (mPFC), (C) prelimbic–infralimbic cortex (PrL-IL), (D) ventral diagonal band of Broca (VDB), and (E) ventral tegmental area–substantia nigra (VTA/SN). Patterned stimulation of the olfactory bulb was applied at 100 Hz (red curve) and at 20 Hz (blue curve). BOLD signals increased in the mPFC, PrL-IL, and VDB. BOLD responses for each train were normalized to exclude effects due to baseline shifts. Gray boxes indicate the stimulation period. A significant difference between stimulation protocols is marked with a black asterisk (\*) and significant BOLD responses with a red (100 Hz protocol) or blue (20 Hz protocol) asterisk.

a broad range of patterned stimulation protocols, including HFS, all of which lead to synaptic plasticity of different magnitudes, durations, and directions in the hippocampus, do not generate synaptic plasticity in the aPC of freely behaving rats (Strauch and Manahan-Vaughan 2018). By contrast, we found that the more complex and prolonged HFS protocol, used in the current study, triggers OB–aPC LTP that lasts for over 4 h. This 100 Hz protocol consisted of a total of 2000 pulses that were applied in a pattern over a 20-min time-period and resulted successfully in LTP. In contrast, in our previous study, HFS failed to induce synaptic plasticity with a protocol consisting of 100 Hz applied as 400 pulses in four trains of each 100 pulses, and an intertrain interval of 5 min (Strauch and Manahan-Vaughan 2018). Several studies *in vitro* and *in vivo* support that the degree and duration of synaptic potentiation or depression is dependent not only on the afferent frequency used but also on the number of pulses and the stimulation pattern (Manahan-Vaughan 2000; Hernandez et al. 2005; Buschler et al. 2012). The duration and complexity of the 100 Hz HFS protocol used in the present study may have been decisive for LTP induction, compared with the lack of complexity

of our previously tested 100 Hz protocol and/or lower frequency of the 20 Hz protocol used in the present study, which failed to induce LTP. In line with this, others have shown that very prolonged stimulation of the lateral olfactory tract results in LTP in the aPC (Racine et al. 1983).

### Detection of Odor Processing in Rodent Brain Using fMRI

We did not explore the direct effect of odor presentation in our study, on the one hand, because others have reported that odor stimuli only elicit minor BOLD signal changes (Poplawsky and Kim 2014) and on the other hand, because detection of signals typically requires a much higher field strength than could be generated by the 4.7 Tesla magnet used in our study (Han et al. 2019; Muir et al. 2019). In general, cerebral blood volume–weighted fMRI appears to be more sensitive to odor exposure than BOLD fMRI for the detection of signal changes in the OB (Poplawsky and Kim 2014). Although stimulation of the lateral olfactory tract changes BOLD responses in the OB, it is more difficult to ascribe signals precisely to OB layers, compared with cerebral blood volume–weighted fMRI (Poplawsky et al. 2015). Only a few studies examined regions beyond the OB and rostral olfactory cortex regions in rodents (Kulkarni et al. 2012; Han et al. 2019; Muir et al. 2019). In awake rats, odor presentation results in changes in BOLD responses in several brain regions, whereby the hippocampus, limbic cortex, AON, and tenia tecta are activated in an odor-specific manner (Kulkarni et al. 2012). In anesthetized mice, blood volume–weighted fMRI also revealed a differentiated response of brain regions to the presentation of a monomolecular, compared with a conspecific, odor (Muir et al. 2019). Here, the IL–PrL reacted strongest to the conspecific odor, whereas the piriform cortex reacted more strongly to the monomolecular odor (Muir et al. 2019). For our study, we combined electrical stimulation with fMRI, which is well-established for the hippocampus (Angenstein et al. 2007, 2009, 2010; Canals et al. 2009; Krautwald and Angenstein 2012). These studies support that changes in BOLD response are dependent on the input activity, but also depend on processing in the neuronal circuitry that is examined (Angenstein et al. 2010). Interpreted in light of the findings of the odor studies mentioned above, it is tempting to speculate that the HFS protocol used in our study emulated complex (conspecific), rather than monomolecular, odor processing.

### Influence of Sedation on Neurotransmission

Medetomidine mildly suppressed basal synaptic transmission without hindering the induction of synaptic plasticity in our study. The magnitude of change in the evoked responses generated by LTP induction, 1) in the presence of medetomidine, 2) after the animal subsequently recovered from sedation, and 3) in an experiment where the animals could freely move, was equivalent in all cases. Medetomidine is a selective  $\alpha_2$ -adrenergic receptor agonist (Stenberg et al. 1987). These receptors are presynaptic and act by inhibiting adenylyl cyclase, suppressing  $\text{Ca}^{2+}$  entry into presynaptic terminals and by increasing  $\text{K}^{+}$ -mediated hyperpolarization (Hayashi and Maze 1993). As a result, neurotransmission is bridled without being completely suppressed. In line with this, at the dosage used in our study, we saw no strong effects of medetomidine on basal synaptic transmission.

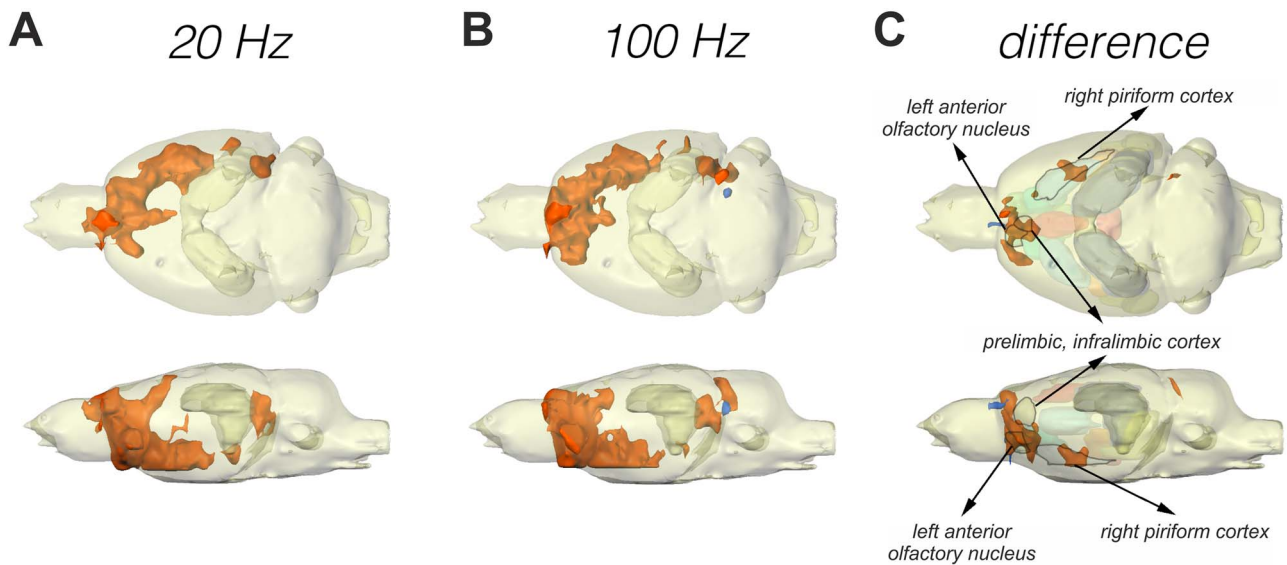


**Figure 7.** GLM and second-level analysis showing activated voxels during patterned stimulation of the olfactory bulb that correspond to regions of the olfactory system and associated brain regions. (A–C) The 3D activation map depicts results of general linear model (GLM) analysis to detect all significantly activated voxels (increase in activation: orange; decrease in activation: blue) during application of (A) 20 Hz and (B) 100 Hz stimulation to the olfactory bulb. (C) A second-level analysis (difference) was performed to map significantly different BOLD responses between the two stimulation protocols (orange: significantly stronger activation with 100 Hz stimulation; blue: significantly stronger activation with 20 Hz stimulation). BOLD responses of the left AON and areas of the right piriform cortex are significantly stronger during 100 Hz, compared with 20 Hz, stimulation applied to the olfactory bulb. VOIs that showed a significant difference between stimulation protocols in the VOI analysis (see Figs 3–6) are labeled and marked by an outline to depict an overlap between VOI analysis and the second-level analysis. All other analyzed VOIs (volumes of interest) are displayed in a transparent manner.

### Relationship of Electrophysiological Stimulation of the Olfactory Bulb to Olfactory Information Processing

The duration and pattern of stimulation used in our study raise the question as to what extent this kind of activity can be expected to occur under physiological conditions. In anesthetized mice, the membrane potential of mitral cells, the output of the OB, changes with the respiration rate and, upon odor presentation, bursts of action potentials are elicited during each breathing cycle (Margrie and Schaefer 2003; Schaefer and Margrie 2007). In awake rats, the respiration rate, at rest, has a frequency of 1–2 Hz (similar to the 1 Hz frequency in each train of our 100 Hz protocol), whereas active sniffing, for example, during odor sampling occurs at rates above 4 Hz up to 12 Hz (Welker 1964; Wachowiak 2011). An amplification in the amplitude of oscillations in the beta frequency range (15–40 Hz) occurs in trained animals, indicating that this frequency may occur during recognition memory (Ravel et al. 2003; Martin et al. 2004; Martin et al. 2006). The 20 Hz stimulation pattern that we used, and which did not trigger synaptic plasticity in the aPC, lies within the range of frequencies recorded from the OB when it samples an odor (15–30 Hz) (Kay et al. 1996). We previously reported that stimulation of the OB with a similar frequency (25 Hz) does not affect basal evoked responses and does not trigger synaptic plasticity (Strauch and Manahan-Vaughan 2018). In agreement with our previous result, we could not induce synaptic plasticity in the aPC with 20 Hz stimulation of the OB. This would suggest that frequencies in the range of odor sampling applied (in a simple pattern) only to the OB do not typically result in synaptic information encoding. However, the lack of complexity of the 20 Hz stimulation protocol used may have contributed to the failure of induction of synaptic plasticity in the aPC. Earlier studies described the ability of rats to discriminate unilateral

stimulation at different sites within the OB, or along the lateral olfactory tract, as well as following multisite OB stimulation (Mouly et al. 1985; Mouly and Holley 1986; Roman et al. 1987). Furthermore, olfactory discrimination learning can be enhanced by OB stimulation (Cohen et al. 2015), and learning enhances evoked responses in the piriform cortex (Roman et al. 1987, 1993; Cohen et al. 2015). These reports raise the possibility that stimulation at multiple sites in the OB, or the application of a more complex pattern of 20 Hz stimulation, may change synaptic efficacy in the aPC.

A study by Carey and Wachowiak (2011) examined effects of a sniff playback combined with odor presentation on OB output neurons. That study detected peak firing rates between 40 and 200 Hz (mean: 115 and 103 Hz for different anesthetics) and a duration of spiking activity of either ca. 66 ms or ca. 175 ms (Laing 1986; Carey and Wachowiak 2011; Wachowiak 2011). Thus, the frequency of 100 Hz, as well as the duration of each burst (200 ms), we applied here to trigger aPC LTP is likely to be generated physiologically in the OB. It has been shown that rodents and humans are able to discriminate odors already after a single sniff (Uchida and Mainen 2003) and a go/no-go training task can be learned in ca. 120 trials that includes learning of odor sampling (Martin et al. 2004). Acquisition of a simple odor discrimination task can be achieved as early as within 10–20 trials that requires sniffing at two different wells (Linster and Hasselmo 1999; Cleland et al. 2002). This corresponds to a time-span of less than 20 min (Linster and Hasselmo 1999). These results suggest that the more complex and longer stimulation pattern (100 Hz) we applied here could be similar to activity induced in the OB over the time course of the learning of an odor discrimination task. This experience may thus be stored by means of synaptic plasticity in the aPC.

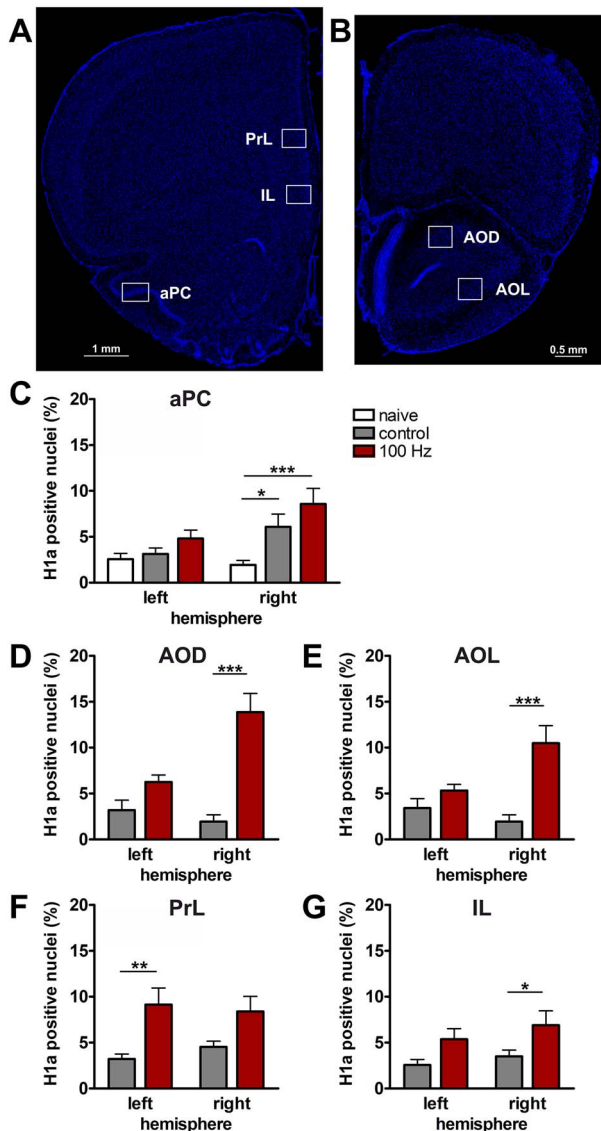


**Figure 8.** 100 Hz stimulation of the olfactory bulb results in an increase in nuclear Homer1a mRNA expression in olfactory cortex and associated brain regions. (A, B) DAPI-stained coronal sections of a rat brain showing regions of interest (white rectangles) in one of the analyzed hemispheres. (A) Sections for prelimbic cortex (PrL), infralimbic cortex (IL), and anterior piriform cortex (aPC) were obtained between +3.0 and +3.5 mm anterior to bregma. (B) For the dorsal (AOD) and lateral (AOL) anterior olfactory nucleus, sections between +5.0 and +5.5 mm anterior to bregma were analyzed. (C–G) Plots showing the relative percentage of nuclear Homer1a (H1a) mRNA expression in (C) aPC, (D) AOD, (E) AOL, (F) PrL, and (G) IL in the left (unstimulated) and right (stimulated) hemispheres of naive (only aPC; white bars), test-pulse stimulated control (gray bars), and 100 Hz stimulated animals (red bars). (C) In the aPC, 100 Hz stimulation of the right OB results in an increase in Homer1a expression in the right aPC compared with the left aPC of all three groups (post hoc test: right 100 Hz: vs. left naive  $P < 0.01$ ; vs. left control  $P < 0.01$ ; vs. left 100 Hz  $P < 0.05$ ) and the right aPC of the naive group (post hoc test:  $P < 0.001$ ). Test-pulse stimulation of the right OB resulted in an increase in Homer1a mRNA expression in the right aPC (control) compared with the left and right hemisphere of the naive animals (post hoc test: right control: vs. left naive  $P < 0.05$ ; vs. right naive  $P < 0.05$ ). (D, E) In AOD and AOL, the right AOD and AOL exhibit a significant elevation of Homer1a expression following 100 Hz stimulation compared with the left AOD and AOL of the same group (post hoc test: AOD:  $P < 0.01$ ; AOL:  $P < 0.05$ ), as well as left and right AOD and AOL of the control group (AOD right 100 Hz: vs. right control  $P < 0.0001$ ; vs. left control:  $P < 0.0001$ ; AOL right 100 Hz: vs. right control  $P < 0.001$ ; vs. left control:  $P < 0.01$ ). (F) In the PrL, 100 Hz stimulation increases Homer1a mRNA expression

## A Putative Connectome for Odor Information Processing

During 20 Hz stimulation of the OB, we detected significant changes in BOLD signals in the AON, piriform cortex, PrL, IL, dorsal medial prefrontal cortex, VDB, nucleus accumbens, BLA, and entorhinal cortex. This finding is in agreement with anatomical studies of OB projections (White 1965; Price 1973). The AON sends feedback and centrifugal projections to the ipsilateral and contralateral OB and sends afferents to the piriform and orbitofrontal cortices (Haberly and Price 1978; Illig and Eudy 2009; Cleland and Linster 2019). It receives inputs from the OB, piriform, and entorhinal cortices (Cleland and Linster 2019). The AON may be involved in the bilateral integration of odor information and serve as a relay for neuromodulatory information to the OB (Rothermel and Wachowiak 2014).

We detected significant Homer1a elevations in the ipsilateral IL, but not ipsilateral PrL after HFS of the OB. The PrL and IL receive olfactory information via olfactory cortex regions such as AON, tenia tecta, and piriform cortex (Luskin and Price 1983; Conde et al. 1995; Hoover and Vertes 2007; Diodato et al. 2016; Moberly et al. 2018). Interesting in this regard is the fact that the PrL, but not the IL, receives inputs from the entorhinal cortex and orbitofrontal cortices (Hoover and Vertes 2007). Taken together, different olfactory input weights from these regions to PrL and IL may be the reason for the different IEG expression patterns detected in these structures in our study. Although a tendency toward significant Homer1a expression was detected in the PrL ipsilateral to HFS (compared with test-pulse stimulated controls), effects were significant in the contralateral PrL. This opens up the interesting possibility of bilateral olfactory information processing by the PrL. Anatomically, this may be enabled by contralateral projections between the anterior olfactory nuclei (Illig and Eudy 2009) and their respective direct afferent projections to the PrL (Ahmed et al. 1995; Moberly et al. 2018). Contralateral communication between the prelimbic cortices may also facilitate this process (Gemmell and O'Mara 2000; Vertes 2004).

The entorhinal cortex is another known element of the olfactory system (Price 1973; Haberly and Price 1978; Luskin and Price 1983). It plays a role in sensory information processing (Knierim et al. 2014; Li et al. 2017) and in odor working memory, and activity in single neurons reflects different phases of a trial in a delayed nonmatching to sample task (Young et al. 1997; Egorov et al. 2002). Cholinergic inputs from the basal forebrain that project via the VDB (de Olmos et al. 1978; Diodato et al. 2016; Mazo et al. 2017) alter odor coding in the OB (Rothermel et al. 2014), whereas the nucleus accumbens, dorsal striatum, dorsomedial prefrontal cortex, and the BLA are involved in context-dependent processing of aversive or pleasant outcomes related to odor experience (Rolls et al. 2003; Schoenbaum and Setlow 2003; Walker et al. 2005; Grabenhorst et al. 2007; Atallah et al. 2008; Prehn-Kristensen et al. 2009;

in both hemispheres compared with the left PrL of control animals (post hoc test left control: vs. right 100 Hz  $P < 0.05$ ; vs. left 100 Hz  $P < 0.01$ ), and, also in the left hemisphere of stimulated animals compared with the right PrL of controls (post hoc test:  $P < 0.05$ ). (G) By contrast, only the right IL shows a significantly higher percentage of Homer1a mRNA-positive neurons after 100 Hz stimulation in comparison to the left and right IL of the control group (post hoc test right 100 Hz: vs. left control  $P < 0.05$ ; vs. right control  $P < 0.05$ ). C–G: mean  $\pm$  SEM. Significant differences between naive, control, and test groups within either left or right hemisphere, revealed by post hoc analysis (Fisher's LSD test), are marked with asterisks: \* $P < 0.05$ , \*\* $P < 0.01$ , \*\*\* $P < 0.001$ .

Cousens et al. 2011; Kim et al. 2014; Floresco 2015; Davies et al. 2017). These regions also exhibit increases in beta frequency oscillatory activity during odor processing and recognition (Martin et al. 2006; Chapuis et al. 2009). Our fMRI results show that when the OB is activated, all of these structures are active, suggesting their concomitant involvement in odor experience evaluation.

In addition to the identification of structures that are activated by information transmission from the OB, we also identified structures that are specifically activated when the OB triggers LTP in the aPC. Here, we first identified these structures using fMRI and then their role in somatic gene encoding was subsequently assessed using a fluorescence in situ hybridization approach that is temporally constrained (Bottai et al. 2002; Vazdarjanova et al. 2002; Hoang et al. 2018). This latter approach allows us to specifically identify those neurons that engaged in information encoding, presumably to enable long-term retention of the experience (Hoang et al. 2018). Using the same method, regions of the olfactory cortex have been reported to exhibit odor-specific changes in the expression of various immediate early genes (Bepari et al. 2012). The stimulation frequency (100 Hz) used to trigger LTP in our study is in the range of frequencies detected in the OB during odor association and learning (65–100 Hz) (Kay et al. 1996; Ravel et al. 2003; Beshel et al. 2007). We detected significantly higher BOLD activity in the IL, PrL, PC, and AON as a result of 100 Hz compared with 20 Hz stimulation. All of these structures also exhibited significant elevations in somatic immediate early gene expression as a result of 100 Hz stimulation.

Interestingly, both test-pulse and 100 Hz stimulation of the OB enhanced immediate early gene expression in the aPC of the stimulated hemisphere, when compared with Homer1a expression in naive animals. For the OB, an increase in c-Fos and Arg3.1 mRNA expression upon novel odor presentation has been described, whereas exposure to a familiar odor results in lower levels of mRNA expression (Montag-Sallaz and Buonviso 2002). Moreover, repetitive odor stimulation results in a habituation of neuronal responses in OB and aPC (Wilson 1998). Given that monomolecular odor processing triggers significant signal processing in the piriform cortex (Muir et al. 2019), one possible explanation is that test-pulse stimulation emulated novel monomolecular information processing in this structure and thus triggered immediate early gene expression. By contrast, 100 Hz HFS might emulate more complex odor processing that is associated with information encoding by means of synaptic plasticity. But there is a caveat in attempting to make a direct comparison between our immediate early gene and electrophysiological results: Evoked responses, including LTP, were recorded in (dendritic) layer 1 of the aPC, whereas immediate early gene expression was analyzed in semilunar and superficial pyramidal cells of layer 2, where cell soma are located. Semilunar cells receive their main input from the OB, whereas the OB input to superficial pyramidal cells is much weaker (Franks and Isaacson 2006; Bathellier et al. 2009; Suzuki and Bekkers 2011). Thus, it is likely that semilunar cells were the main instigator of LTP in the aPC in our study. In our immediate early gene analysis, a selective increase in activity in semilunar cells (triggered by HFS) might have been masked to some extent by the inevitable inclusion of both principal cell types in layer 2. Conversely, associative inputs or selective inputs to superficial pyramidal cells of layer 2 may have supported IEG expression in response to test-pulse stimulation in the absence of a corresponding change in synaptic strength in

layer 1. In line with this possibility, it has been reported that the AON only poorly innervates semilunar cells (Hagiwara et al. 2012). Furthermore, whereas responses in semilunar cells are predominantly driven by information flow from the OB, activity in superficial pyramidal cells is modulated by recurrent corticocortical inputs (Hagiwara et al. 2012).

The possibility also exists that antidromic relay could have contributed to the response changes that we detected following OB stimulation. Antidromic relay from the piriform cortex to the LOT and OB has been described in different experimental preparations (Willey et al. 1975; Uva et al. 2006) and might serve to transiently amplify signal transmission from the LOT to the aPC. Stimulation of the PC can trigger antidromic responses in the orbitofrontal cortex (Cinelli et al. 1987) that could also serve to reinforce aPC responses and information encoding. This might explain why the relatively weak test-pulse stimulation of the OB resulted in gene encoding in the aPC.

### Involvement of Prelimbic and Infralimbic Cortices in Odor Information Processing

Our finding that the IL and PrL exhibit enhanced immediate early gene expression levels upon HFS of the OB, consistent with experience encoding, was unexpected. The IL and PrL are best known for their contributions to the encoding, regulation, and suppression of aversive experience, particularly in the context of extinction learning (Giustino and Maren 2015; Izquierdo et al. 2016; Lingawi et al. 2019). But the PrL has also been implicated in goal-directed behavior and the coupling of context with action (Hok et al. 2005; Rich and Shapiro 2009; Mukherjee and Caroni 2018; Woon et al. 2020). It also supports cue attention (Sharpe and Killcross 2014). The IL enables both flexibility in, and habitual, behavior (Barker et al. 2014) and may be involved in visceromotor control (Vertes 2006).

Very few studies have addressed the role of the PrL or IL in odor information processing: Rouillet and colleagues reported increases in Fos immunoreactivity in rats that were either trained in an odor-association task or were simply exposed to unreinforced odor cues (Rouillet et al. 2005). Beside other regions, they revealed the increase in Fos immunoreactivity in the IL but they did not scrutinize the PrL. However, a reaction of the PrL and IL to conspecific odors has been reported (Muir et al. 2019) and Nikaido and Nakashima reported distinct single-unit activity patterns in the IL and PrL of freely behaving rats in response to anxiolytic and anxiogenic odors (Nikaido and Nakashima 2011). This suggests that these structures may modulate odor-response behaviors in a valence-based manner. In line with this possibility, it has been shown that blockade of N-methyl-D-aspartate receptors in the PrL prevents odor-reward associative learning (Tronel and Sara 2003) and the PrL has been implicated in avoidance behavior linked to predator odors (Hwa et al. 2019). Our findings offer novel insights into the involvement of the PrL and IL in odor information processing: We not only see strong BOLD responses during activation of the OB but triggering of OB-aPC LTP also results in somatic gene encoding in the PrL and IL. This indicates that these structures play an intrinsic role in odor-experience encoding. Viewed from the perspective of the above-mentioned findings and the anatomical wiring of the PrL and IL with motor, reward-modulating, and limbic structures (Shipman et al. 2019; Wood et al. 2019), this role may comprise the determination of behavioral responses to odor experience.

## Conclusions

In this study, we describe a subcortical and cortical information processing and encoding system that engages during information transmission from the OB. The portfolio of structures that were identified as being part of this system suggests that odor detection by the OB is typically accompanied by odor valence evaluation. Thus, in addition to olfactory structures such as the AON, PC, and entorhinal cortex, the nucleus accumbens, dorsal striatum, medial prefrontal cortex, PrL, IL, VDB, and BLA were all activated during OB information processing. The nucleus accumbens is involved in the processing of motivation, aversion, reward, and reinforcement learning (Floresco 2015). The BLA, IL, and PrL are involved in the encoding and the modification of responses to context-dependent experience. Given that both the IL (Sesack et al. 1989; Hurley et al. 1991; Vertes 2004) and the PC send afferents to the nucleus accumbens (Wright et al. 1996; Schwabe et al. 2004), the medial prefrontal cortex instructs the dorsal striatum (Davies et al. 2017) and the PrL and IL influence information processing in the BLA, we propose that the connectome we identified in our study may contribute to odor valence evaluation. Furthermore, finding that induction of LTP in OB-aPC synapses results in somatic gene encoding in the PrL, IL, and AON raises the possibility that patterns of activity in the OB can generate neural signatures that target, via the aPC, structures that engage in valence-specific information processing. The aPC projects back to the OB (Diodato et al. 2016; Mazo et al. 2017) thus, also creating the possibility that under specific conditions dialog between these two structures reinforces, or indeed alters, information processing.

Taken together, the findings of our study support that the olfactory system works in close conjunction with reward and aversion-encoding systems of the brain in the rapid processing and long-term encoding of OB stimuli. The recruitment of these nonolfactory structures is likely to play a key role in the evaluation of the valence of odor experience.

## Supplementary Material

Supplementary material can be found at *Cerebral Cortex* online.

## Funding

This project was supported by a grant from the German Research Foundation (Deutsche Forschungsgemeinschaft, [www.dfg.de](http://www.dfg.de); SFB874/B1, project number: 122679504 to D.M.-V.).

## Notes

We gratefully thank Karla Krautwald, Juliane Boege, Ute Neubacher, Beate Krenzke, and Jens Colitti-Klausnitzer for technical assistance. We thank Nadine Kolloesch for animal care. *Conflict of Interest*: None.

## Author Contributions Statement

The experiments were designed by D.M.-V. and C.S. with contributions from F.A.; fMRI: F.A. and C.S.; electrophysiology: C.S.; and in situ hybridization: C.S. and T.H.H.; D.M.-V. wrote the paper, with contributions from all authors.

## References

- Adams JC. 1992. Biotin amplification of biotin and horseradish peroxidase signals in histochemical stains. *J Histochem Cytochem.* 40:1457–1463.
- Ahmed AK, Dong K, Sugioka K, Yamadori T. 1995. Afferent projections to the cingulate cortex in albino rats: a study with a retrograde labeling method using fluoro-gold. *Kobe J Med Sci.* 41:247–255.
- Angenstein F, Kammerer E, Niessen HG, Frey JU, Scheich H, Frey S. 2007. Frequency-dependent activation pattern in the rat hippocampus, a simultaneous electrophysiological and fMRI study. *Neuroimage.* 38:150–163.
- Angenstein F, Kammerer E, Scheich H. 2009. The BOLD response in the rat hippocampus depends rather on local processing of signals than on the input or output activity. A combined functional MRI and electrophysiological study. *J Neurosci.* 29:2428–2439.
- Angenstein F, Krautwald K, Scheich H. 2010. The current functional state of local neuronal circuits controls the magnitude of a BOLD response to incoming stimuli. *Neuroimage.* 50:1364–1375.
- Atallah HE, Rudy JW, O'Reilly RC. 2008. The role of the dorsal striatum and dorsal hippocampus in probabilistic and deterministic odor discrimination tasks. *Learn Mem.* 15:294–298.
- Barker JM, Taylor JR, Chandler LJ. 2014. A unifying model of the role of the infralimbic cortex in extinction and habits. *Learn Mem.* 21:441–448.
- Bathellier B, Margrie TW, Larkum ME. 2009. Properties of piriform cortex pyramidal cell dendrites: implications for olfactory circuit design. *J Neurosci.* 29:12641–12652.
- Bepari AK, Watanabe K, Yamaguchi M, Tamamaki N, Takebayashi H. 2012. Visualization of odor-induced neuronal activity by immediate early gene expression. *BMC Neurosci.* 13:140.
- Beshel J, Kopell N, Kay LM. 2007. Olfactory bulb gamma oscillations are enhanced with task demands. *J Neurosci.* 27:8358–8365.
- Bottai D, Guzowski JF, Schwarz MK, Kang SH, Xiao B, Lanahan A, Worley PF, Seeburg PH. 2002. Synaptic activity-induced conversion of intronic to exonic sequence in Homer 1 immediate early gene expression. *J Neurosci.* 22:167–175.
- Bovet-Carmona M, Krautwald K, Menigoz A, Vennekens R, Balschun D, Angenstein F. 2019. Low frequency pulse stimulation of Schaffer collaterals in Trpm4(−/−) knockout rats differently affects baseline BOLD signals in target regions of the right hippocampus but not BOLD responses at the site of stimulation. *Neuroimage.* 188:347–356.
- Brakeman PR, Lanahan AA, O'Brien R, Roche K, Barnes CA, Huganir RL, Worley PF. 1997. Homer: a protein that selectively binds metabotropic glutamate receptors. *Nature.* 386:284–288.
- Buschler A, Goh JJ, Manahan-Vaughan D. 2012. Frequency dependency of NMDA receptor-dependent synaptic plasticity in the hippocampal CA1 region of freely behaving mice. *Hippocampus.* 22:2238–2248.
- Calu DJ, Roesch MR, Stalnaker TA, Schoenbaum G. 2007. Associative encoding in posterior piriform cortex during odor discrimination and reversal learning. *Cereb Cortex.* 17:1342–1349.
- Canals S, Beyerlein M, Merkle H, Logothetis NK. 2009. Functional MRI evidence for LTP-induced neural network reorganization. *Curr Biol.* 19:398–403.
- Carey RM, Wachowiak M. 2011. Effect of sniffing on the temporal structure of mitral/tufted cell output from the olfactory bulb. *J Neurosci.* 31:10615–10626.

- Cavarsan CF, Tescarollo F, Tesone-Coelho C, Morais RL, Motta FL, Blanco MM, Mello LE. 2012. Pilocarpine-induced status epilepticus increases Homer1a and changes mGluR5 expression. *Epilepsy Res.* 101:253–260.
- Chapuis J, Garcia S, Messaoudi B, Thevenet M, Ferreira G, Gervais R, Ravel N. 2009. The way an odor is experienced during aversive conditioning determines the extent of the network recruited during retrieval: a multisite electrophysiological study in rats. *J Neurosci.* 29:10287–10298.
- Chapuis J, Wilson DA. 2011. Bidirectional plasticity of cortical pattern recognition and behavioral sensory acuity. *Nat Neurosci.* 15:155–161.
- Cinelli AR, Ferreyra-Moyano H, Barragan E. 1987. Reciprocal functional connections of the olfactory bulbs and other olfactory related areas with the prefrontal cortex. *Brain Res Bull.* 19:651–661.
- Cleland TA, Linster C. 2019. Central olfactory structures. *Handb Clin Neurol.* 164:79–96.
- Cleland TA, Morse A, Yue EL, Linster C. 2002. Behavioral models of odor similarity. *Behav Neurosci.* 116:222–231.
- Cohen Y, Wilson DA, Barkai E. 2015. Differential modifications of synaptic weights during odor rule learning: dynamics of interaction between the piriform cortex with lower and higher brain areas. *Cereb Cortex.* 25:180–191.
- Conde F, Maire-Lepoivre E, Audinat E, Crepel F. 1995. Afferent connections of the medial frontal cortex of the rat. II. Cortical and subcortical afferents. *J Comp Neurol.* 352:567–593.
- Cousens GA, Skrobacz CG, Blumenthal A. 2011. Nucleus accumbens carbachol disrupts olfactory and contextual fear-potentiated startle and attenuates baseline startle reactivity. *Behav Brain Res.* 216:673–680.
- Davies DA, Greba Q, Selk JC, Catton JK, Baillie LD, Mulligan SJ, Howland JG. 2017. Interactions between medial prefrontal cortex and dorsomedial striatum are necessary for odor span capacity in rats: role of GluN2B-containing NMDA receptors. *Learn Mem.* 24:524–531.
- de Olmos J, Hardy H, Heimer L. 1978. The afferent connections of the main and the accessory olfactory bulb formations in the rat: an experimental HRP-study. *J Comp Neurol.* 181:213–244.
- Diodato A, Ruinat de Brimont M, Yim YS, Derian N, Perrin S, Pouch J, Klatzmann D, Garel S, Choi GB, Fleischmann A. 2016. Molecular signatures of neural connectivity in the olfactory cortex. *Nat Commun.* 7:12238.
- Doty FD, Entzminger G, Kulkarni J, Pamarthy K, Staab JP. 2007. Radio frequency coil technology for small-animal MRI. *NMR Biomed.* 20:304–325.
- Egorov AV, Hamam BN, Fransén E, Hasselmo ME, Alonso AA. 2002. Graded persistent activity in entorhinal cortex neurons. *Nature.* 420:173–178.
- Floresco SB. 2015. The nucleus accumbens: an interface between cognition, emotion, and action. *Annu Rev Psychol.* 66:25–52.
- Franks KM, Isaacson JS. 2006. Strong single-fiber sensory inputs to olfactory cortex: implications for olfactory coding. *Neuron.* 49:357–363.
- Gemmell C, O'Mara SM. 2000. Long-term potentiation and paired-pulse facilitation in the prelimbic cortex of the rat following stimulation in the contralateral hemisphere in vivo. *Exp Brain Res.* 132:223–229.
- Giustino TF, Maren S. 2015. The role of the medial prefrontal cortex in the conditioning and extinction of fear. *Front Behav Neurosci.* 9:298.
- Grabehorst F, Rolls ET, Margot C, da Silva MA, Velazco MI. 2007. How pleasant and unpleasant stimuli combine in different brain regions: odor mixtures. *J Neurosci.* 27:13532–13540.
- Guzowski JF, Worley PF. 2001. Cellular compartment analysis of temporal activity by fluorescence in situ hybridization (catFISH). *Curr Protoc Neurosci.* 15:1.8.1–1.8.16. doi: [10.1002/0471142301.ns0108s15](https://doi.org/10.1002/0471142301.ns0108s15).
- Haberly LB, Price JL. 1978. Association and commissural fiber systems of the olfactory cortex of the rat. *J Comp Neurol.* 178:711–740.
- Hagiwara A, Pal SK, Sato TF, Wienisch M, Murthy VN. 2012. Optophysiological analysis of associational circuits in the olfactory cortex. *Front Neural Circuits.* 16:18.
- Han Z, Chen W, Chen X, Zhang K, Tong C, Zhang X, Li CT, Liang Z. 2019. Awake and behaving mouse fMRI during go/no-go task. *Neuroimage.* 188:733–742.
- Hansen N, Manahan-Vaughan D. 2015. Locus Coeruleus stimulation facilitates long-term depression in the dentate gyrus that requires activation of beta-adrenergic receptors. *Cereb Cortex.* 25:1889–1896.
- Hayashi Y, Maze M. 1993. Alpha 2 adrenoceptor agonists and anaesthesia. *Br J Anaesth.* 71:108–118.
- Helbing C, Angenstein F. 2020. Frequency-dependent electrical stimulation of fimbria-fornix preferentially affects the mesolimbic dopamine system or prefrontal cortex. *Brain Stimul.* 13:753–764.
- Hennig J, Nauerth A, Friedburg H. 1986. RARE imaging: a fast imaging method for clinical MR. *Magn Reson Med.* 3:823–833.
- Hernandez RV, Navarro MM, Rodriguez WA, Martinez JL Jr, LeBaron RG. 2005. Differences in the magnitude of long-term potentiation produced by theta burst and high frequency stimulation protocols matched in stimulus number. *Brain Res Brain Res Protoc.* 15:6–13.
- Hoang TH, Aliane V, Manahan-Vaughan D. 2018. Novel encoding and updating of positional, or directional, spatial cues are processed by distinct hippocampal subfields: evidence for parallel information processing and the “what” stream. *Hippocampus.* 28:315–326.
- Hoang TH, Boge J, Manahan-Vaughan D. 2021. Hippocampal subfield-specific Homer1a expression is triggered by learning-facilitated long-term potentiation and long-term depression at medial perforant path synapses. *Hippocampus.* doi: [10.1002/hipo.23333](https://doi.org/10.1002/hipo.23333).
- Hok V, Save E, Lenck-Santini PP, Poucet B. 2005. Coding for spatial goals in the prelimbic/infralimbic area of the rat frontal cortex. *Proc Natl Acad Sci USA.* 102:4602–4607.
- Hoover WB, Vertes RP. 2007. Anatomical analysis of afferent projections to the medial prefrontal cortex in the rat. *Brain Struct Funct.* 212:149–179.
- Hurley KM, Herbert H, Moga MM, Saper CB. 1991. Efferent projections of the infralimbic cortex of the rat. *J Comp Neurol.* 308:249–276.
- Hwa LS, Neira S, Pina MM, Pati D, Calloway R, Kash TL. 2019. Predator odor increases avoidance and glutamatergic synaptic transmission in the prelimbic cortex via corticotropin-releasing factor receptor 1 signaling. *Neuropsychopharmacology.* 44:766–775.
- Illig KR, Eudy JD. 2009. Contralateral projections of the rat anterior olfactory nucleus. *J Comp Neurol.* 512:115–123.
- Izquierdo I, Furini CR, Myskiw JC. 2016. Fear memory. *Physiol Rev.* 96:695–750.

- Kay LM, Lancaster LR, Freeman WJ. 1996. Reafference and attractors in the olfactory system during odor recognition. *Int J Neural Syst.* 7:489–495.
- Kim H, Kim TK, Kim JE, Park JY, Lee Y, Kang M, Kim KS, Han PL. 2014. Adenylyl cyclase-5 in the dorsal striatum function as a molecular switch for the generation of behavioral preferences for cue-directed food choices. *Mol Brain.* 7:77.
- Knierim JJ, Neunuebel JP, Deshmukh SS. 2014. Functional correlates of the lateral and medial entorhinal cortex: objects, path integration and local-global reference frames. *Philos Trans R Soc Lond B Biol Sci.* 369:20130369.
- Krautwald K, Angenstein F. 2012. Low frequency stimulation of the perforant pathway generates anesthesia-specific variations in neural activity and BOLD responses in the rat dentate gyrus. *J Cereb Blood Flow Metab.* 32:291–305.
- Kulkarni P, Stolberg T, Sullivanjr JM, Ferris CF. 2012. Imaging evolutionarily conserved neural networks: preferential activation of the olfactory system by food-related odor. *Behav Brain Res.* 230:201–207.
- Laing DG. 1986. Identification of single dissimilar odors is achieved by humans with a single sniff. *Physiol Behav.* 37:163–170.
- Lehallier B, Rampin O, Saint-Albin A, Jerome N, Ouali C, Maurin Y, Bonny JM. 2012. Brain processing of biologically relevant odors in the awake rat, as revealed by manganese-enhanced MRI. *PLoS One.* 7:e48491.
- Li B, Gong L, Wu R, Li A, Xu F. 2014. Complex relationship between BOLD-fMRI and electrophysiological signals in different olfactory bulb layers. *Neuroimage.* 95:29–38.
- Li Y, Xu J, Liu Y, Zhu J, Liu N, Zeng W, Huang N, Rasch MJ, Jiang H, Gu X, et al. 2017. A distinct entorhinal cortex to hippocampal CA1 direct circuit for olfactory associative learning. *Nat Neurosci.* 20:559–570.
- Lingawi NW, Laurent V, Westbrook RF, Holmes NM. 2019. The role of the basolateral amygdala and infralimbic cortex in (re)learning extinction. *Psychopharmacology (Berl).* 236:303–312.
- Linster C, Hasselmo ME. 1999. Behavioral responses to aliphatic aldehydes can be predicted from known electrophysiological responses of mitral cells in the olfactory bulb. *Physiol Behav.* 66:497–502.
- Luskin MB, Price JL. 1983. The topographic organization of associational fibers of the olfactory system in the rat, including centrifugal fibers to the olfactory bulb. *J Comp Neurol.* 216:264–291.
- Manahan-Vaughan D. 2000. Long-term depression in freely moving rats is dependent upon strain variation, induction protocol and behavioral state. *Cereb Cortex.* 10:482–487.
- Margrie TW, Schaefer AT. 2003. Theta oscillation coupled spike latencies yield computational vigour in a mammalian sensory system. *J Physiol.* 546:363–374.
- Marr D. 1971. Simple memory: a theory for archicortex. *Philos Trans R Soc Lond B Biol Sci.* 262:23–81.
- Martin C, Gervais R, Hugues E, Messaoudi B, Ravel N. 2004. Learning modulation of odor-induced oscillatory responses in the rat olfactory bulb: a correlate of odor recognition? *J Neurosci.* 24:389–397.
- Martin C, Gervais R, Messaoudi B, Ravel N. 2006. Learning-induced oscillatory activities correlated to odour recognition: a network activity. *Eur J Neurosci.* 23:1801–1810.
- Martin C, Grenier D, Thevenet M, Vigouroux M, Bertrand B, Janier M, Ravel N, Litaudon P. 2007. fMRI visualization of transient activations in the rat olfactory bulb using short odor stimulations. *Neuroimage.* 36:1288–1293.
- Martin C, Ravel N. 2014. Beta and gamma oscillatory activities associated with olfactory memory tasks: different rhythms for different functional networks? *Front Behav Neurosci.* 8:218.
- Mazo C, Grimaud J, Shima Y, Murthy VN, Lau CG. 2017. Distinct projection patterns of different classes of layer 2 principal neurons in the olfactory cortex. *Sci Rep.* 7:8282.
- Moberly AH, Schreck M, Bhattarai JP, Zweifel LS, Luo W, Ma M. 2018. Olfactory inputs modulate respiration-related rhythmic activity in the prefrontal cortex and freezing behavior. *Nat Commun.* 9:1528.
- Montag-Sallaz M, Buonviso N. 2002. Altered odor-induced expression of c-fos and arg 3.1 immediate early genes in the olfactory system after familiarization with an odor. *J Neurobiol.* 52:61–72.
- Mouly AM, Holley A. 1986. Perceptive properties of the multi-site electrical microstimulation of the olfactory bulb in the rat. *Behav Brain Res.* 21:1–12.
- Mouly AM, Vigouroux M, Holley A. 1985. On the ability of rats to discriminate between microstimulations of the olfactory bulb in different locations. *Behav Brain Res.* 17:45–58.
- Muir ER, Biju KC, Cong L, Rogers WE, Torres Hernandez E, Duong TQ, Clark RA. 2019. Functional MRI of the mouse olfactory system. *Neurosci Lett.* 704:57–61.
- Mukherjee A, Caroni P. 2018. Infralimbic cortex is required for learning alternatives to pre-learned associations through reciprocal connectivity. *Nat Commun.* 9:2727.
- Nikaido Y, Nakashima T. 2011. Different patterns of neuronal activities in the infralimbic and prelimbic cortices and behavioral expression in response to two affective odors, 2,5-dihydro-2,4,5-trimethylthiazoline and a mixture of cis-3-hexenol and trans-2-hexenal, in the freely moving rat. *Behav Brain Res.* 218:218–227.
- Oliveira VC, Carrara RC, Simoes DL, Saggioro FP, Carlotti CG Jr, Covas DT, Neder L. 2010. Sudan Black B treatment reduces autofluorescence and improves resolution of in situ hybridization specific fluorescent signals of brain sections. *Histol Histopathol.* 25:1017–1024.
- Paxinos G, Watson C. 2014. *Paxino's and Watson's the rat brain in stereotaxic coordinates.* Amsterdam; Boston: Elsevier/AP, Academic Press is an imprint of Elsevier.
- Poplawsky AJ, Fukuda M, Murphy M, Kim SG. 2015. Layer-specific fMRI responses to excitatory and inhibitory neuronal activities in the olfactory bulb. *J Neurosci.* 35:15263–15275.
- Poplawsky AJ, Kim SG. 2014. Layer-dependent BOLD and CBV-weighted fMRI responses in the rat olfactory bulb. *Neuroimage.* 91:237–251.
- Potschka H, Krupp E, Ebert U, Gumbel C, Leichtlein C, Lorch B, Pickert A, Kramps S, Young K, Grune U, et al. 2002. Kindling-induced overexpression of Homer 1A and its functional implications for epileptogenesis. *Eur J Neurosci.* 16:2157–2165.
- Prehn-Kristensen A, Wiesner C, Bergmann TO, Wolff S, Jansen O, Mehdorn HM, Ferstl R, Pause BM. 2009. Induction of empathy by the smell of anxiety. *PLoS One.* 4:e5987.
- Price JL. 1973. An autoradiographic study of complementary laminar patterns of termination of afferent fibers to the olfactory cortex. *J Comp Neurol.* 150:87–108.
- Qu LP, Kahnt T, Cole SM, Gottfried JA. 2016. De novo emergence of odor category representations in the human brain. *J Neurosci.* 36:468–478.
- Racine RJ, Milgram NW, Hafner S. 1983. Long-term potentiation phenomena in the rat limbic forebrain. *Brain Res.* 260:217–231.

- Ravel N, Chabaud P, Martin C, Gaveau V, Hugues E, Tallon-Baudry C, Bertrand O, Gervais R. 2003. Olfactory learning modifies the expression of odour-induced oscillatory responses in the gamma (60–90 Hz) and beta (15–40 Hz) bands in the rat olfactory bulb. *Eur J Neurosci*. 17:350–358.
- Rich EL, Shapiro M. 2009. Rat prefrontal cortical neurons selectively code strategy switches. *J Neurosci*. 29:7208–7219.
- Roesch MR, Stalnaker TA, Schoenbaum G. 2007. Associative encoding in anterior piriform cortex versus orbitofrontal cortex during odor discrimination and reversal learning. *Cereb Cortex*. 17:643–652.
- Rolls ET, Kringelbach ML, de Araujo IE. 2003. Different representations of pleasant and unpleasant odours in the human brain. *Eur J Neurosci*. 18:695–703.
- Roman FS, Chaillan FA, Soumireu-Mourat B. 1993. Long-term potentiation in rat piriform cortex following discrimination learning. *Brain Res*. 601:265–272.
- Roman F, Staubli U, Lynch G. 1987. Evidence for synaptic potentiation in a cortical network during learning. *Brain Res*. 418:221–226.
- Rothermel M, Carey RM, Puche A, Shipley MT, Wachowiak M. 2014. Cholinergic inputs from Basal forebrain add an excitatory bias to odor coding in the olfactory bulb. *J Neurosci*. 34:4654–4664.
- Rothermel M, Wachowiak M. 2014. Functional imaging of cortical feedback projections to the olfactory bulb. *Front Neural Circuits*. 8:73.
- Roulet F, Datiche F, Lienard F, Cattarelli M. 2005. Learning-stage dependent Fos expression in the rat brain during acquisition of an olfactory discrimination task. *Behav Brain Res*. 157:127–137.
- Saar D, Grossman Y, Barkai E. 1998. Reduced after-hyperpolarization in rat piriform cortex pyramidal neurons is associated with increased learning capability during operant conditioning. *Eur J Neurosci*. 10:1518–1523.
- Schaefer AT, Margrie TW. 2007. Spatiotemporal representations in the olfactory system. *Trends Neurosci*. 30:92–100.
- Schafer JR, Kida I, Rothman DL, Hyder F, Xu F. 2005. Adaptation in the rodent olfactory bulb measured by fMRI. *Magn Reson Med*. 54:443–448.
- Schindelin J, Arganda-Carreras I, Frise E, Kaynig V, Longair M, Pietzsch T, Preibisch S, Rueden C, Saalfeld S, Schmid B, et al. 2012. Fiji: an open-source platform for biological-image analysis. *Nat Methods*. 9:676–682.
- Schoenbaum G, Chiba AA, Gallagher M. 1998. Orbitofrontal cortex and basolateral amygdala encode expected outcomes during learning. *Nat Neurosci*. 1:155–159.
- Schoenbaum G, Chiba AA, Gallagher M. 1999. Neural encoding in orbitofrontal cortex and basolateral amygdala during olfactory discrimination learning. *J Neurosci*. 19:1876–1884.
- Schoenbaum G, Eichenbaum H. 1995. Information coding in the rodent prefrontal cortex. II. Ensemble activity in orbitofrontal cortex. *J Neurophysiol*. 74:751–762.
- Schoenbaum G, Setlow B. 2003. Lesions of nucleus accumbens disrupt learning about aversive outcomes. *J Neurosci*. 23:9833–9841.
- Schwabe K, Ebert U, Loscher W. 2004. The central piriform cortex: anatomical connections and anticonvulsant effect of GABA elevation in the kindling model. *Neuroscience*. 126:727–741.
- Sesack SR, Deutch AY, Roth RH, Bunney BS. 1989. Topographical organization of the efferent projections of the medial prefrontal cortex in the rat: an anterograde tract-tracing study with Phaseolus vulgaris leucoagglutinin. *J Comp Neurol*. 290:213–242.
- Sethumadhavan N, Hoang TH, Strauch C, Manahan-Vaughan D. 2020. Involvement of the Postrhinal and Perirhinal cortices in microscale and macroscale visuospatial information encoding. *Front Behav Neurosci*. 14. doi: [10.3389/fnbeh.2020.556645](https://doi.org/10.3389/fnbeh.2020.556645).
- Sharpe MJ, Killcross S. 2014. The prelimbic cortex contributes to the down-regulation of attention toward redundant cues. *Cereb Cortex*. 24:1066–1074.
- Shipman ML, Johnson GC, Bouton ME, Green JT. 2019. Chemo-genetic silencing of prelimbic cortex to anterior dorsomedial striatum projection attenuates operant responding. *eNeuro*. 6. doi: [10.1523/ENEURO.0125-19.2019](https://doi.org/10.1523/ENEURO.0125-19.2019).
- Stalnaker TA, Cooch NK, McDannald MA, Liu TL, Wied H, Schoenbaum G. 2014. Orbitofrontal neurons infer the value and identity of predicted outcomes. *Nat Commun*. 5:3926.
- Stenberg D, Salven P, Miettinen MV. 1987. Sedative action of the alpha 2-agonist medetomidine in cats. *J Vet Pharmacol Ther*. 10:319–323.
- Strauch C, Manahan-Vaughan D. 2018. In the piriform cortex, the primary impetus for information encoding through synaptic plasticity is provided by descending rather than ascending olfactory inputs. *Cereb Cortex*. 28:764–776.
- Strauch C, Manahan-Vaughan D. 2020. Orchestration of hippocampal information encoding by the piriform cortex. *Cereb Cortex*. 30:135–147.
- Suzuki N, Bekkers JM. 2011. Two layers of synaptic processing by principal neurons in piriform cortex. *J Neurosci*. 31:2156–2166.
- Tronel S, Sara SJ. 2003. Blockade of NMDA receptors in prelimbic cortex induces an enduring amnesia for odor-reward associative learning. *J Neurosci*. 23:5472–5476.
- Uchida N, Mainen ZF. 2003. Speed and accuracy of olfactory discrimination in the rat. *Nat Neurosci*. 6:1224–1229.
- Uva L, Strowbridge BW, de Curtis M. 2006. Olfactory bulb networks revealed by lateral olfactory tract stimulation in the in vitro isolated Guinea-pig brain. *Neuroscience*. 142:567–577.
- Vazdarjanova A, McNaughton BL, Barnes CA, Worley PF, Guzowski JF. 2002. Experience-dependent coincident expression of the effector immediate-early genes arc and Homer 1a in hippocampal and neocortical neuronal networks. *J Neurosci*. 22:10067–10071.
- Vertes RP. 2004. Differential projections of the infralimbic and prelimbic cortex in the rat. *Synapse*. 51:32–58.
- Vertes RP. 2006. Interactions among the medial prefrontal cortex, hippocampus and midline thalamus in emotional and cognitive processing in the rat. *Neuroscience*. 142:1–20.
- Wachowiak M. 2011. All in a sniff: olfaction as a model for active sensing. *Neuron*. 71:962–973.
- Walker DL, Paschall GY, Davis M. 2005. Glutamate receptor antagonist infusions into the basolateral and medial amygdala reveal differential contributions to olfactory vs. context fear conditioning and expression. *Learn Mem*. 12:120–129.
- Welker W. 1964. Analysis of sniffing of the albino rat. *Behaviour*. 22:223–244.
- White LE. 1965. Olfactory bulb projections of the rat. *Anat Rec*. 152:465–480.
- Willey TJ, Maeda G, Rafuse D. 1975. Antidromic unit in the prepyriform cortex driven by olfactory peduncular volleys. *Brain Res*. 92:132–136.
- Wilson DA. 1998. Habituation of odor responses in the rat anterior piriform cortex. *J Neurophysiol*. 79:1425–1440.

- Wilson DA, Hoptman MJ, Gerum SV, Guilfoyle DN. 2011. State-dependent functional connectivity of rat olfactory system assessed by fMRI. *Neurosci Lett.* 497:69–73.
- Wood M, Adil O, Wallace T, Fourman S, Wilson SP, Herman JP, Myers B. 2019. Infralimbic prefrontal cortex structural and functional connectivity with the limbic forebrain: a combined viral genetic and optogenetic analysis. *Brain Struct Funct.* 224:73–97.
- Woon EP, Sequeira MK, Barbee BR, Gourley SL. 2020. Involvement of the rodent prelimbic and medial orbitofrontal cortices in goal-directed action: a brief review. *J Neurosci Res.* 98:1020–1030.
- Wright CI, Beijer AV, Groenewegen HJ. 1996. Basal amygdaloid complex afferents to the rat nucleus accumbens are compartmentally organized. *J Neurosci.* 16:1877–1893.
- Xu F, Kida I, Hyder F, Shulman RG. 2000. Assessment and discrimination of odor stimuli in rat olfactory bulb by dynamic functional MRI. *Proc Natl Acad Sci USA.* 97:10601–10606.
- Yang X, Renken R, Hyder F, Siddeek M, Greer CA, Shepherd GM, Shulman RG. 1998. Dynamic mapping at the laminar level of odor-elicited responses in rat olfactory bulb by functional MRI. *Proc Natl Acad Sci USA.* 95:7715–7720.
- Young BJ, Otto T, Fox GD, Eichenbaum H. 1997. Memory representation within the parahippocampal region. *J Neurosci.* 17:5183–5195.
- Zhao F, Wang X, Zariwala HA, Uslaner JM, Houghton AK, Evelhoch JL, Hostetler E, Winkelmann CT, Hines CDG. 2017. fMRI study of the role of glutamate NMDA receptor in the olfactory adaptation in rats: insights into cellular and molecular mechanisms of olfactory adaptation. *Neuroimage.* 149:348–360.
- Zhao F, Wang X, Zariwala HA, Uslaner JM, Houghton AK, Evelhoch JL, Williams DS, Winkelmann CT. 2016. fMRI study of olfaction in the olfactory bulb and high olfactory structures of rats: insight into their roles in habituation. *Neuroimage.* 127:445–455.
- Zhu J, Hafycz J, Keenan BT, Guo X, Pack A, Naidoo N. 2020. Acute sleep loss upregulates the synaptic scaffolding protein, Homer1a, in non-canonical sleep/wake brain regions, claustrum, piriform and cingulate cortices. *Front Neurosci.* 14:188.
- Zucker RS, Regehr WG. 2002. Short-term synaptic plasticity. *Annu Rev Physiol.* 64:355–405.